


RESEARCH ARTICLE OPEN ACCESS

Allergy and Inflammation

KIRA6 is an Effective and Versatile Mast Cell Inhibitor of IgE-mediated Activation

Veronika Wunderle^{1,2}  | Thomas Wilhelm¹ | Shatha Boukeileh³ | Jonas Goßen⁴ | Michael A. Margreiter⁴ | Roman Sakurov¹ | Sandro Capellmann¹ | Maike Schwoerer¹ | Nabil Ahmed¹ | Gina Bronneberg¹ | Michel Arock⁵ | Christian Martin⁶ | Thomas Schubert⁷ | Francesca Levi-Schaffer³ | Giulia Rossetti^{4,8,9} | Boaz Tirosh^{3,10} | Michael Huber¹

¹Institute of Biochemistry and Molecular Immunology, Medical Faculty, RWTH Aachen University, Aachen, Germany | ²Department of Neurology, Faculty of Medicine and University Hospital Cologne, University of Cologne, Cologne, Germany | ³The School of Pharmacy, The Hebrew University of Jerusalem, Jerusalem, Israel | ⁴Institute for Advanced Simulation, Jülich Supercomputing Centre, Forschungszentrum Jülich GmbH, Jülich, Germany | ⁵Department of Hematological Biology, Pitié-Salpêtrière Charles-Foix Hospital, AP-HP Sorbonne University, Paris, France | ⁶Institute of Pharmacology and Toxicology, Medical Faculty, RWTH Aachen University, Aachen, Germany | ⁷2bind, Regensburg, Germany | ⁸Jülich Supercomputing Centre (JSC), Forschungszentrum Jülich GmbH, Jülich, Germany | ⁹Department of Neurology, University Hospital Aachen, RWTH Aachen University, Aachen, Germany | ¹⁰Department of Biochemistry, Case Western Reserve University, Cleveland, Ohio, USA

Correspondence: Michael Huber (mhuber@ukaachen.de)

Received: 28 June 2024 | **Revised:** 12 November 2024 | **Accepted:** 21 November 2024

Funding: The research was funded by grants from the German-Israeli Foundation for Scientific Research and Development (grant no. I-1471-414.13/2018) to M.H., B.T., and F.L.S.

Keywords: allergy treatment | IgE | inflammation | mast cells | signal transduction

ABSTRACT

Mast cell (MC)-driven allergic diseases are constantly expanding and require the development of novel pharmacological MC stabilizers. Allergen/antigen (Ag)-triggered activation via crosslinking of the high-affinity receptor for IgE (FcεRI) is fundamentally regulated by SRC family kinases, for example, LYN and FYN, exhibiting positive and negative functions. We report that KIRA6, an inhibitor for the endoplasmic reticulum stress sensor IRE1α, suppresses IgE-mediated MC activation by inhibiting both LYN and FYN. KIRA6 attenuates Ag-stimulated early signaling and effector functions such as degranulation and proinflammatory cytokine production/secretion in murine bone marrow-derived MCs. Moreover, Ag-triggered bronchoconstriction in an ex vivo model and IgE-mediated stimulation of human MCs were repressed by KIRA6. The interaction of KIRA6 with three MC-relevant tyrosine kinases, LYN, FYN, and KIT, and the potential of KIRA6 structure as a pharmacophore for the development of respective single-, dual-, or triple-specificity inhibitors, was evaluated by homology modeling and molecular dynamics simulations. We found that KIRA6 particularly strongly binds the inactive state of LYN, FYN, and KIT with comparable affinities. In conclusion, our data suggest that the chemical structure of KIRA6 as a pharmacophore can be further developed to obtain an effective MC stabilizer.

1 | Introduction

Pharmacological modulation of enzymatic activities of signaling proteins, such as protein and lipid kinases, has become a gen-

eral practice in the treatment of inflammatory and neoplastic diseases [1, 2]. Particularly in the latter, cells frequently develop resistance to the drug used, amongst others, by directly acquiring mutations in the drug target rendering it inaccessible to the drug,

Veronika Wunderle and Thomas Wilhelm contributed equally to this study.

This is an open access article under the terms of the [Creative Commons Attribution](https://creativecommons.org/licenses/by/4.0/) License, which permits use, distribution and reproduction in any medium, provided the original work is properly cited.

© 2024 The Author(s). *European Journal of Immunology* published by Wiley-VCH GmbH.

or by the induction/activation of additional signaling proteins leading to the re-structuring of whole signaling pathways [3, 4]. Consequently, a second or third drug should be administered to regain treatment success. Drugs with the potential to inhibit different enzymes, preferentially in structurally or kinetically different pathways, should reduce the development of resistance mechanisms. Similar points would account for inflammatory diseases, for example, allergic hypersensitivity diseases. Here, not the development of drug-resistant cells, but the insufficiency of only one drug to control different aspects of the activation of one or more cell types involved would pose limitations. Especially in allergies or other mast cell (MC)-mediated diseases, the combined blockade of initial, receptor-proximal activation processes as well as the kinetically downstream production of a multitude of mediators, such as cytokines and chemokines, with the potential to activate further inflammatory cells, would be desirable.

A central mechanism of allergic MC activation is initiated by the antigen/allergen (Ag)-mediated cross-linking of the IgE-loaded high-affinity receptor for IgE (FcεRI) and subsequent induction of various signaling pathways eventually resulting in typical MC responses such as degranulation (release of preformed mediators from secretory lysosomes) and production of lipid mediators as well as proinflammatory cytokines (e.g., IL-6 and TNF) [5]. A crucial signaling enzyme in FcεRI-mediated MC activation is the SRC family kinase (SFK) LYN, which constitutively interacts with the FcεRI β-chain [6]. After receptor cross-linking, LYN phosphorylates the tyrosine (Tyr) residues in the immunoreceptor Tyr-based activation motives of the FcεRI β- and γ-chains, allowing for consequent interaction with SH2-domain-containing proteins thus initiating differential signaling pathways necessary for MC activation, for example, phospholipase Cγ (PLCγ), phosphatidylinositol-3-kinase (PI3K), and mitogen-activated protein kinases (MAPKs) controlled processes [5].

Once PLCγ is recruited to the plasma membrane, particularly by the transmembrane adaptor protein LAT1 (Linker for activated T cells 1), it hydrolyzes its substrate phosphatidylinositol-4,5-bisphosphate (PI4,5P₂) to yield inositol-1,4,5-trisphosphate (IP₃) and diacylglycerol (DAG) [5]). Whereas DAG promotes activation of conventional and novel isotypes of PKC, IP₃ binds to its receptor in the membrane of the endoplasmic reticulum (ER), which results in the release of Ca²⁺ from the ER and eventually in the STIM1/ORAI1-controlled influx of extracellular Ca²⁺ [7]. Both Ca²⁺ influx and PKC activation are mandatory for the process of degranulation [8, 9]. PI3K and MAPKs are particularly involved in transcriptional processes relevant to the production of proinflammatory cytokines [5]. Inhibition of signaling processes in the course of allergic MC activation, preferably close to the initial activating event (e.g., LYN activation), would be desirable. However, assigning only activating or inhibitory functions to a protein is hard in the context of cellular signaling, since activators can be initiators of negative feedback mechanisms as well [10]. LYN, for instance, can phosphorylate and activate the lipid phosphatase SH2-domain-containing inositol 5'-phosphatase 1 (SHIP1), a dominant negative regulator of the PI3K pathway, which hydrolyzes the PI3K-generated phospholipid phosphatidylinositol-3,4,5-trisphosphate (PI3,4,5P₃) [11, 12]. Moreover, LYN is engaged in the attenuation of further SFKs, such as FYN, by contributing to the activation of the C-terminal

SRC kinase (CSK), which then phosphorylates SFKs at their inhibitory, C-terminal Tyr residue allowing for intramolecular SH2-domain/phospho-Tyr interaction [5].

Both proliferating and secreting cells are particularly dependent on ER-mediated translation of proteins involving accurate folding and assembly of effective complexes while still in the lumen of the ER. An elaborate control system has evolved, called the unfolded protein response (UPR), which detects unfolded/misfolded proteins and activates cellular mechanisms to relieve folding stress (adaptive UPR) [13]. Three sensor proteins in the membrane of the ER detect such unfolded proteins hence resulting in the activation of sensor-specific transcription factors that allow adaptation to this cellular stress by activating genes involved in ER expansion, protein folding, and aggregate degradation, amongst others [14]. These sensors are inositol-requiring enzyme 1α (IRE1α), protein kinase RNA-like ER kinase (PERK), and activating transcription factor 6 (ATF6), with IRE1α being the evolutionary oldest. IRE1α comprises a luminal N-terminal binding immunoglobulin protein/heat shock protein 5 (BIP/HSPA5)-binding domain, a central cytoplasmic serine/threonine (Ser/Thr) kinase domain, and a C-terminal ribonuclease (RNase) domain. The presence of misfolded proteins causes the chaperone-BIP to dissociate from IRE1α causing its oligomerization, autophosphorylation, and activation of the RNase domain [14]. Active IRE1α RNase then nonconventionally splices the mRNA of the transcription factor X-box binding protein 1 (XBP1), allowing its stable translation, nuclear translocation, and transcription of genes involved in adaptive UPR. Excess folding stress overburdens the adaptive UPR and switches it, promoted by the stress sensor PERK, to a terminal response (apoptosis) [14].

The development of various small molecule inhibitors against the three UPR sensors has allowed the unraveling of differential functions of the UPR [15]. Moreover, the dependence on an effective UPR system of tumor cells holds great promise for the use of such inhibitors in cancer therapy. In recent years, however, cross-reactive proteins of certain UPR inhibitors were identified, which were even more sensitive to the respective inhibitor than the initial target [16, 17]. In this study, we have found that the IRE1α inhibitor KIRA6 (kinase inhibitor and RNase attenuator 6) [18] is a potent inhibitor of the SFKs LYN and FYN, thus effectively blocking IgE-mediated MC activation. In-depth molecular modeling analysis revealed enhanced affinity of KIRA6 for the inactive conformations of the catalytic centers of LYN, FYN, and KIT. Thus, the structure of KIRA6 might offer a promising pharmacophore for the development of novel anti-allergy MC stabilizers.

2 | Material and Methods

2.1 | Cell culture, cell lines, and IgE sensitization

Murine bone marrow-derived mast cells (BMMCs) from WT or mutant mice deficient for SHIP1 (gene name: *Inpp5d*) (*Ship1*^{-/-}) or LYN (*Lyn*^{-/-}) were generated as described previously [19] from 6- to 8-week-old mice (littermates, mixed C57BL/6×129/Sv background).

Hematopoietic bone marrow stem cells were cultured in RPMI 1640 medium + L-glutamine (Thermo Fisher Scientific, #21875-034) containing 1% X63Ag8-653-conditioned medium (source of IL-3), 15% FCS (Capricorn, #FCS-12A), 10 mM HEPES (Sigma-Aldrich, #H0887), 100 μ M β -mercaptoethanol (Sigma-Aldrich, #M6250), 100 units/mL penicillin and 100 μ g/mL streptomycin (Sigma-Aldrich, #P0781). After a differentiation period of 4–6 weeks, >95% of the cells were KIT⁺ and Fc ϵ RI-positive confirming successful MC differentiation.

BMMCs were sensitized for Ag stimulation with dinitrophenol (DNP) coupled to human serum albumin (HSA) (DNP-HSA, Sigma-Aldrich, #A6661) by pre-loading the Fc ϵ RI with 0.15 μ g/mL IgE (clone SPE-7, Sigma-Aldrich, #A2831) overnight. If starvation was indicated, the culture medium was replaced by a medium containing 10% FCS and lacking IL-3, 12–16 h before the experiment.

Experiments with BMMCs were performed in the laboratory of M.H. All experiments were performed in accordance with German legislation governing animal studies and following the Principles of Laboratory Animal Care. Mice are held in the Institute of Laboratory Animal Science, Medical Faculty of RWTH Aachen University, which holds a license for husbandry and breeding of laboratory animals from the Veterinary Office of the Staedteregion Aachen (Administrative District). The Institute follows a Quality Management System, which is certified according to DIN ISO 9001/2015. Every step in this project involving mice was reviewed by the animal welfare officer. All experiments were approved by the Landesamt für Natur, Umwelt und Verbraucherschutz NRW (LANUV), Recklinghausen (AZ 84-02.04.2016.A496).

The mast cell leukemia cell line HMC-1.2 (KIT^{V560G, D816V}), kindly provided by Dr. J. Butterfield (Mayo Clinic) [20], was cultured in RPMI 1640 medium (Thermo Fisher Scientific, #21875-034) supplemented with 10% FCS (Capricorn, #FCS-12A) and 100 units/mL penicillin + 100 μ g/mL streptomycin (Sigma-Aldrich, #P0781) in a humidified atmosphere containing 5% CO₂. The medium was renewed twice a week.

ROSA^{KIT WT} cells were cultured as previously described (Saleh et al., 2014) in IMDM medium (Thermo Fisher Scientific, #21980-032) supplemented with 100 units penicillin/mL and 100 μ g/mL streptomycin (Sigma-Aldrich, #P0781), 1 mM sodium pyruvate (Thermo Fisher Scientific, #11360-039), MEM vitamin solution (Thermo Fisher Scientific, #11120-037), MEM amino acids (Thermo Fisher Scientific, #11130-036), 2 mM L-glutamine (Thermo Fisher Scientific, #25030-024), Insulin-Transferrin-Selenium (Thermo Fisher Scientific, #41400-045), 100 μ M β -mercaptoethanol (Sigma-Aldrich, #M6250), 0.1% BSA (Serva, #11930.04), and 80 ng/mL mSCF from CHO culture supernatant [21].

ROSA^{KIT WT} cells were primed for 4 days with rh-IL-4 (20 ng/mL; ImmunoTools, #1134B0045) and human monoclonal IgE (2 μ g/mL; Sigma-Aldrich, #401152) to enhance the expression of the Fc ϵ RI before stimulation [22].

Human cord blood-derived MCs (CBMCs) were obtained by culturing umbilical cord blood mononuclear cells as previously

described [23]. In brief, fresh cord blood diluted in Hank's solution was loaded on Lymphoprep (Serumwerk Bernburg, #1858) and centrifuged (350 \times g, 25 min, 24°C). Mononuclear cells were washed twice and resuspended in a minimum essential medium containing 10 μ g/mL ribonucleases (MEM- α nucleosides; Gibco, #12571063) supplemented with 10% heat-inactivated FCS (HyClone, GE Healthcare, SV30160.03), 100 U/mL penicillin and 100 μ g/mL streptomycin (Gibco, #15140-122) and containing recombinant human stem cell factor (h-SCF; Gibco, PeproTech, #300-07; 100 ng/mL) and human IL-6 (Gibco, PeproTech, #200-06; 20 ng/mL). Prostaglandin E2 (PGE2; Sigma-Aldrich, #P0409; 1 ng/mL) was also regularly added in order to prevent any monocytic development. Cells were maintained in a humidified incubator (37°C, 5% CO₂) with media replaced on a weekly basis. Following a 7–8-week culture period, CBMCs were used following examination for maturity and viability. Experiments with CBMCs were performed in the laboratory of F.L.S. Cord blood was obtained according to the Institutional Helsinki Committee guidelines of Hadassah Hospital, and its use was approved by the committee.

For activation of CBMCs, human myeloma IgE (0.3 μ g/mL, Sigma-Aldrich, #401152) was used for sensitizing the cells in the presence of recombinant human IL-4 (Gibco, PeproTech, #200-04; 10 ng/mL) for 3 days. Subsequently, cells were washed twice and resuspended in Tyrode's buffer (consisting of 137 mM NaCl, 5.5 mM glucose, 2 mM KCl, 12 mM NaHCO₃, and 0.3 mM Na₂HPO₄, supplemented with 1.8 mM CaCl₂ and 0.9 mM MgCl₂; pH 7.34 for a short stimulation of 30 min) or in a CBMC medium supplemented with recombinant h-SCF (100 ng/mL, Gibco, PeproTech, #300-07) (for a longer stimulation). CBMCs were activated with polyclonal rabbit anti-human IgE Ab (5 μ g/mL, Dako, #A0094).

2.2 | Materials

KIRA6 was purchased from Cayman Chemical (#19151). KIRA8 (#SML2903), A23187 (#C7522), Dinitrophenol-human serum albumin (DNP-HSA, #A6661), and monoclonal IgE with specificity for DNP (clone Spe-7, Sigma, #A2831) were from Sigma Aldrich. Murine SCF was from PeproTech (#250-03). PMA (#1585) came from Sigma-Aldrich and Thapsigargin (TG, #ab147487) from Abcam. Saracatinib (#S1006) was purchased from Selleckchem and Tunicamycin (#A2242) from Applchem. DMSO (#4720.1) was obtained from Carl Roth GmbH & Co.

2.3 | Calcium Measurement

BMMCs were preloaded with IgE and starved (10% FCS, no IL-3) overnight. Cells were resuspended at a density of 1×10^7 cells/mL in RPMI 1640 containing 1% FCS, 0.1% BSA (Serva, #11930.04), 1.3 μ M Fluo-3 AM (#F1241), 2.7 μ M Fura Red AM (#F3020), and 0.1% Pluronic F-127 (all ThermoFisher) and incubated for 45 min at 37°C for flow cytometry analysis in a FACSCalibur flow cytometer (BD Biosciences). Steady-state fluorescence was measured for 1 min before 20 ng/mL DNP-HSA were added for 4 min. Subsequently, the ratios of the Ca²⁺-bound/Ca²⁺-unbound were used to generate line graphs from FACS profiles using the

FlowJo analysis software (Treestar) and normalized areas under the curve were calculated for objectification.

2.4 | ELISAs

To determine IL-6 and TNF secretion, murine BMMCs were stimulated as indicated in the respective experiments. If cells were stimulated with Ag, MCs were preloaded with IgE (clone Spe-7, 0.15 µg/mL). Cell number was adjusted to 1.2×10^6 cells/mL in stimulation medium (RPMI 1640 + 0.1% BSA (Serva, #11930.04), cells were allowed to adapt to 37°C and stimulated for 3 h. Supernatants were collected to determine cytokine release. Ninety-six-well ELISA plates (Corning, #9018) were coated with capturing anti-IL-6 (1:250, BD Biosciences, #554400) or anti-TNF (1:200, R&D Systems, #AF410-NA) antibodies diluted in PBS overnight at 4°C according to manufacturer's instructions. ELISA plates were washed three times with PBS+0.1% Tween and blocked with PBS+2% BSA (IL-6 ELISA) or PBS+1%BSA+5% sucrose (TNF ELISA) before loading of supernatants (50 µL for IL-6 ELISA, 100 µL for TNF ELISA). Additionally, to the loading of supernatants, IL-6 (BD Pharmingen, #554582) and TNF (R&D Systems, #410-MT-010) serial 1:2 standard dilutions were added and plates were incubated overnight at 4°C. Thereupon plates were washed three times again followed by incubation with biotinylated anti-IL-6 (1:500, BD Biosciences, #554402) and anti-TNF (1:250, R&D Systems, #BAF-410) antibodies diluted in PBS+1% BSA for 45 min and 2 h, respectively, at room temperature (RT). After three washing steps, streptavidin alkaline phosphatase (1:1000, BD Pharmingen, #554065) was added for 30 min at RT. After three more washing steps, the substrate *p*-Nitro-phenyl-phosphate (1 pill per 5 mL in sodium carbonate buffer) (2 mM MgCl₂ in 50 mM sodium carbonate, pH 9.8), (Sigma, #S0942-200TAB) was added and OD₄₅₀ was recorded using a plate reader (BioTek Eon). Qualitative differences and similarities between WT and mutant cells were consistent throughout the study. Levels of secreted cytokines varied due to batch-to-batch variations of primary, differentiated cells of different ages and from different mice.

2.5 | RT-qPCR

RNA was extracted from 4×10^6 cells using RNeasy Mini Kit (Qiagen, #74106) according to the manufacturer's instructions. One microgram of RNA was used for reverse transcription using random hexamer primer (Roche, #11034731001) and Omniscript Kit (Qiagen, #205113) as instructed by the manufacturer. Quantitative PCR was performed on a Rotorgene (Qiagen) using the Sybr green reaction mix (Meridian Bioscience, #QT650-05). Expression was normalized to the reference gene *Hprt/HPRT*. Relative expression ratios were calculated according to the ddC_t method [24].

Primer sequences were as follows: *Hprt* fwd GCT GGT GAA AAG GAC CTC T, *Hprt* rev CAC AGG ACT AGA ACA CCT GC; *Il6* fwd TCC AGT TGC CTT CTT GGG AC, *Il6* rev GTG TAA TTA AGC CTC CGA CTT G; *Xbp1s* fwd AAG AAC ACG CTT GGG AAT GG, *Xbp1s* rev CTG CAC CTG CTG CGG Ac.

Human *IL8* fwd CAC TGC GCC AAC ACA GAA AT, *IL8* rev ATG AAT TCT CAG CCC TCT TCA A; human *HPRT* fwd TGA CAC

TGG CAA AAC AAT GCA, *HPRT* rev GGT CCT TTT CAC CAG CAA GCT; human *XBP1s* fwd AAC CAG GAG TTA AGA CAG CGC TT, *XBP1s* rev CTG CAC CTG CTG CGG ACT

2.6 | Degranulation Assays (β-Hexosaminidase and LAMP1 Assay)

To measure degranulation using release of β-hexosaminidase as a readout, non-starved IgE preloaded BMMCs were washed in sterile PBS, resuspended in Tyrode's buffer (130 mM NaCl, 5 mM KCl, 1.4 mM CaCl₂, 1 mM MgCl₂, 5.6 mM glucose, and 0.1% BSA in 10 mM Hepes, pH 7.4) at a density of 1.2×10^6 , adapted to 37°C and stimulated as indicated. The supernatant was collected by centrifugation and the remaining cell pellet was lysed in Tyrode's buffer containing 10% NP-40. Ten microliters of pellet and supernatant were incubated with 50 µL of substrate solution (1.3 mg/mL *p*-Nitrophenyl-N-acetyl-β-D-glucose in 0.1 M sodium citrate, pH 4.5).

The measurement of *p*-nitrophenol, generated by β-hexosaminidase, was done by a spectrophotometric reader (BioTek Eon) at a wavelength of $\lambda = 405$ nm [25]. The amount of degranulation in percent was determined as follows:

$$\text{Degranulation [\%]} = \frac{\text{OD supernatant}}{\text{OD supernatant} + \text{OD lysate}} \times 100.$$

For the LAMP1 assay, IgE preloaded BMMCs were washed in sterile PBS, resuspended in RPMI 1640 containing 0.1% BSA, and adapted to 37°C. Next, the indicated treatment was performed, cells were pelleted, washed in FACS buffer (PBS, 3% FCS, 0.1% sodium azide), and stained with FITC-conjugated anti-LAMP1 antibody (CD107a; BioLegend, #121605) for 25 min at 4°C. LAMP1 externalization was determined by flow cytometry. Data were analyzed and mean fluorescence intensities were calculated using the FlowJo analysis software.

2.7 | Immunoprecipitation and Western Blotting

A total of 20×10^6 BMMCs per condition were starved and preloaded with IgE overnight, washed with PBS, resuspended in RPMI + 0.1% BSA at a density of 10×10^6 , and allowed to adapt to 37°C. Treatment was performed as indicated in the respective figures and figure legends. Cells were then pelleted and lysed in phosphorylation solubilization buffer (0.5% IGEPAL, 1 mM Na₃VO₄, 0.5% sodium desoxycholate, and protease inhibitors (10 µg/mL aprotinin, 4 mg/mL leupeptin, and 1 mM PMSF) for 1 h at 4°C. After normalization for protein content (Pierce BCA protein assay kits, #23227), samples were mixed with Laemmli buffer and boiled for 5 min at 95°C, whole-cell lysates were subjected to SDS-PAGE and subsequent western blot (WB) analysis [26].

After protein transfer, the polyvinylidene difluoride (PVDF) membrane was dried, hydrophilized by methanol, and blocked in PBST (PBS + 0.5% Tween) wash buffer with dry nonfat milk powder (5% milk powder (w/v) in PBS + 0.5% Tween) for 30 min, before incubation with primary antibody diluted according to manufacturer's instructions overnight at 4°C. Thereupon, mem-

branes were washed three times and incubated with horseradish peroxidase (HRP)-coupled secondary antibody diluted in PBS + 0.5% Tween, the membrane was developed with enhanced chemiluminescence solution using a LAS 4000mini (FujiFilm). The expression of p85, HSP90, or GAPDH served as a control for comparable loading. Since the stimulation times were short (less than 15 min), differences in expression between these loading controls and the analyzed (phospho-)proteins were not expected. Densitometric analysis of the obtained data was performed using ImageJ software (ImageJ, version 1.52a).

For immunoprecipitation, protein-adjusted whole-cell lysates were incubated with the indicated antibody overnight at 4°C under continuous agitation. Then, 25 µL packed protein G-Sepharose beads (GE Healthcare, #GE17-0618-01) were added for 2 h at 4°C under continuous agitation. Beads were pelleted (500×g, 5 min) and supernatants were removed. The beads were washed in diluted (1/5) lysis buffer thoroughly and the precipitates were separated by SDS-PAGE and analyzed by immunoblotting as described above.

The following antibodies were used:

PI3K p85 (CST, #42925); HSP90 (CST, #4877); p-PLCγ1 (Tyr783) (CST, #14008); p-PKB (Ser473) (CST, #4051); p-JNK (Thr183/Tyr185) (CST, #4668); p-MEK1/2 (Thr217, Ser221) (CST, #2338); p-ERK1/2 (Thr202/Tyr204) (CST #4370); p-Tyr100 (CST, #9411) p-IκBα (Ser32) (CST, #2859); IκBα (CST, #9242) p-c-Kit (Tyr719) (CST, #3391), all purchased from Cell Signaling Technology. GAPDH (#sc-32233); LYN (#sc-7274); SHIP1 (P1C1, #sc-8425); SHIP1 (N1, #sc-6244); GST (#sc-138) were purchased from Santa Cruz Biotechnology.

The supernatant of 4G10 hybridoma cells was used for the detection of phosphorylated tyrosines.

HRP-coupled secondary antibodies against goat (#P044901), mouse (#P0447), and rabbit (#P0448) were from Agilent (Dako).

2.8 | MicroScale Thermophoresis

Protein labeling for MicroScale thermophoresis (MST): The human active protein kinases LYN (ProQinase, #0358-0000-1) and FYN (ProQinase, #0352-0000-1) were labeled using Monolith Protein Labeling Kit RED-TRIS NTA 2nd gen (NanoTemper Technologies, # MO-L018) according to the manufacturer's instructions.

MST binding experiments were carried out with 25 nM Red Tris NTA-labeled FYN in binding buffer (20 mM HEPES pH 8, 100 mM NaCl, 0.05% Tween-20, 1% glycerol, 2% DMSO) with a range of concentrations of KIRA6 (200 µM to 6.1 nM) at 40% MST (medium) power, 20% LED power in premium capillaries on a Monolith NT.115 pico device at 25°C (NanoTemper Technologies). Red Tris NTA labeled LYN was studied at 25 nM in binding buffer (20 mM HEPES pH 8, 100 mM NaCl, 0.05% Tween-20, 1% glycerol, 1% DMSO) with a range of concentrations of KIRA6 (100 µM to 3.05 nM) at 60% MST (high) power, 20% LED power in premium capillaries. Data were analyzed using MO. Affinity analysis software (version v2.3, NanoTemper Technologies) at the

standard MST-on time of 30 s. Data fits possessing amplitudes >5 units combined with signal-to-noise levels >5 units were defined as binding events. Aggregation was not observed in the experiments. In order to calculate the fraction bound, the ΔF_{norm} value of each point is divided by the amplitude of the fitted curve, resulting in values from 0 to 1 (0 = unbound, 1 = bound), and processed using the Kaleidagraph software. Error bars represent the standard deviation of two independent experiments (two technical repeats each).

2.9 | Nanodifferential scanning fluorimetry

For modification-free thermal unfolding experiments, FYN or LYN were studied at 800 nM in binding buffer (20 mM HEPES pH 8, 100 mM NaCl, 0.05% Tween-20, 1% glycerol, 1% DMSO) in the absence and presence of KIRA6 (100 µM). Samples were preincubated in high-sensitivity capillaries for 30 min before measurement in the Prometheus NT.48 instrument (NanoTemper Technologies) with 50% sensitivity and a temperature ramp of 1°C/min from 20 to 95°C. Two independent experiments were performed and merged for analysis at 330 nm wavelength using the software PR. StabilityAnalysis (version v1.1, NanoTemper Technologies).

2.10 | In Vitro Kinase Assay

The LYN kinase assay was performed according to the previously described protocol by Laborlette et al. [27]. Briefly, recombinant GST-fusion protein containing SH3P7 was used as an LYN substrate. GST-SH3P7 was recombinantly expressed and purified as described by Brummer et al. [28]. LYN was immunoprecipitated from unstimulated BMMCs with anti-LYN antibodies as previously described [12].

The kinase reaction was performed in the presence of 200 mM ATP with 5 µg SH3P7 and LYN precipitated from 3×10^6 cells for 30 min at RT in 20 µL of kinase buffer containing 40 mM HEPES, pH7.4; 10 mM MgCl₂, 3 mM MnCl₂. DMSO (solvent control) or KIRA6 was preincubated for 10 min at RT before the addition of ATP. The reaction was terminated by adding 2× Laemmli buffer and subsequently, samples were boiled at 95°C for 5 min before being subjected to SDS-PAGE and Western blotting. Phosphorylated SH3P7 was detected by immunostaining using 4G10 antibody.

The IC₅₀ calculator web tool (<https://www.aatbio.com/tools/ic50-calculator>) was used to calculate the IC₅₀ of KIRA6 from the in vitro kinase assay data.

2.11 | Direct Peritonitis Model on Peritoneal Mast Cells

For assessing tryptase levels in the peritoneal cavity, KIRA6 (5 and 10 mg/kg) was administered via intraperitoneal injection in mice 30 min prior to injection of 30 µg/cavity anti-mouse IgE Ab (BioLegend) in 200 µL of PBS, which cross-links FcεRI on peritoneal mast cells. Mice were euthanized 30 min post-IgE injection, peritoneal lavaged with 3 mL cold PBS, and 2 mL on

average were collected. Cells were separated from supernatants by centrifugation and supernatants were cleared by any remaining cell by a second centrifugation step. Trypsase levels were assayed as described before [29]. The trypsin substrate: N-(p-Tosyl)-Gly-Pro-Lys4-nitroanilide acetate (Sigma cat # T-6140) was added to the supernatant and incubated for approximately 1 h. The absorbance was measured in a plate reader at 410 nm. The mouse experiments were performed in the laboratory of F.L.S. (laboratory's permission or accreditation number MD-19-15956-2, investigator's accreditation number 12156) and approved by the Animal Experimentation Ethics Committee of the Hebrew University of Jerusalem and performed in accordance with the guidelines of the committee.

2.12 | Proliferation and Cytotoxicity Tests

2.12.1 | Apoptosis Assay

BMMCs were seeded at a density of 5×10^5 cells/mL and treated with the solvent DMSO or the indicated KIRA6 concentrations for 72 h. After treatment cells were washed and incubated with Annexin V-AlexaFluor 647 (1:100, BioLegend, #640912) in culture medium for 20 min at RT in the dark. Propidium iodide (1 μ g/mL, Sigma, #P4864) was added immediately before analysis by flow cytometry on a FACScanto II (BD Biosciences).

2.12.2 | Proliferation Assays

BMMCs were seeded at a density of 5×10^5 cells/mL and treated with the solvent DMSO or the indicated KIRA6 concentrations for 72 h. After a 24 h treatment, cells were resuspended completely and 50 μ L from each well was diluted in 10 mL PBS for automated multiparameter cell counting using a Casy cell counter (Innovatis) to determine the cell number and viability.

Metabolic activity was measured using the XTT cell proliferation kit II (XTT; Roche, #11465015001). Cells were seeded in microplates at a density of 5×10^5 cells/mL (suspension culture grade, 96 wells, flat bottom) in a final volume of 100 μ L culture medium per well in a humidified atmosphere (37°C, 5% CO₂) for 72 h. After the incubation period, 50 μ L of the XTT labeling mixture was added to each well (final XTT concentration 0.3 mg/mL). Incubation of the microplate was for 3–4 h in a humidified atmosphere (e.g., 37°C, 5% CO₂). The spectrophotometrical absorbance of the samples was measured using a microplate reader. The wavelength used to measure the absorbance of the formazan product of the XTT assay was 475 nm and the reference wavelength was 650 nm. Sample values at 475 nm were subtracted with medium controls (blanked) resulting in delta blanked values. Total absorbance was calculated by subtraction of delta blanked values (475 nm) with their reference values at 650 nm. These absorbance values (A475–A650 nm) are shown in (Figure S7E,F).

2.13 | Molecular Modeling Techniques

The active states of the three kinases were taken from the Protein Data Bank [30] (PDB codes: 1PKG, 2DQ7, and 5XY1 for KIT, FYN,

and LYN, respectively). The inactive state of KIT was available on the PDB (PDB code 6MOB) while no experimentally determined structure of the inactive (DFG-out) states was available for the human LYN and FYN proteins. Therefore, we generated these using the MODELLER software [31].

LYN(DFG-out) homology model: The structure of LYN bound to an inhibitor (PDB_ID: 5XY1) [32] was used as a template with the activation loop deleted (residues: 383–404). The structure of LCK in complex with type 2 inhibitor imatinib was used in the template to model the DFG-out conformation (PDB_ID 2PLO). We generated 100 models, of which the best-scored (DOPE score) [33] structure was used in the following steps.

FYN(DFG-out) homology model: We used the active state crystal structure of FYN (PDB_ID: 2DQ7) [34] as a template for the model. The procedure for the activation loop mimics the one described above for LYN.

Docking of KIRA6 to LYN/FYN/KIT: We docked KIRA6 to the respective proteins with Schrödinger's Glide software [35, 36] in its induced fit mode with standard parameters. We chose the ligand centroids of the homology models and the ligands co-crystallized as the origins for the $10 \times 10 \times 10$ Å inner bounding box.

Molecular dynamics simulations: 200 ns of molecular dynamics trajectories using GROMACS [37] with the AMBER ff99SB-ILDN [38] forcefield were generated. The clustering of the ligand poses was done using the tclust [39] python package. The standard parameters for clustering were used. Alignment was performed on the backbone atoms and the ligand atoms were used for the RMSD calculation. The cluster distance metric was performed using the “ward” metric. The “autocluster” parameter “y” was set to yes, which uses the elbow criterion for cluster number estimation.

Molecular mechanics, general born surface area: The estimation of the binding free energies between KIRA6 binding to the different proteins was performed using the gmx_MMPBSA [40, 41] tool. We removed the PBC conditions for this and used every frame of the last 100 ns after convergence with the parameters igb = 2 and saltcon = 0.15. Additionally, we used the interaction entropy approximation implemented in the tool for the estimation of the conformational entropy. As a comparison, we also calculated the energetics of the cluster representatives with the single point MMGBSA function of the Schrödinger tool suit.

2.14 | Preparation and Use of Precision-Cut Lung Slices

Precision-cut lung slices (PCLS) were prepared from 8-week-old Wistar rats (220 ± 20 g) obtained from Janvier and kept under controlled conditions (22°C, 55% humidity, and 12 h day/night rhythm). Animal care and all experimental procedures were performed according to the rules of the Directive 2010/63/EU of the European Parliament and approved by the ethical committee of the University Hospital Aachen (internal approval-IDs: 80044). Rat PCLS were prepared in the laboratory of C.M. as previously described [42]. Rats were sacrificed by an overdose of pentobar-

bital i.p. (600 mg/kg). Isolated lungs were filled with prewarmed agarose solution (0.75%) via the trachea and subsequently chilled with ice. Then lobes were separated and cut into 5 to 10 mm thick tissue segments from which cores were made along the airways and then cut into $250 \pm 20 \mu\text{m}$ thick slices (Alabama Research and Development). For studies with ovalbumin, the lung slices were incubated overnight with a cell culture medium containing 1% of serum from actively sensitized rats, as previously shown [42]. After overnight culturing, the airways in PCLS were imaged and digitized using a digital video camera. A control picture was taken before the addition of DMSO or KIRA6 and after the addition of ovalbumin (10 $\mu\text{g/mL}$) frames were recorded every 30 s for 15 min. The images were analyzed by the image analysis program Optimas 6.5 (Optimas).

2.15 | Statistics

Data were generated from at least $n = 3$ independent experiments. p -values were calculated as indicated in the respective figure legends using GraphPad Prism. Data are shown as mean \pm SD of $n \geq 3$ independent experiments (with n indicated in the respective figure legends). p -values of * < 0.05 , ** < 0.01 , *** < 0.001 , and **** < 0.0001 were considered statistically significant. Values higher than a p -value of 0.05 were regarded as not significant (ns).

3 | Results

3.1 | KIRA6 Represses Early and Sustained Proinflammatory Functions in Ag-Triggered Mast Cells

The IRE1 α /XBP1 arm of the UPR not only secures the increased need for protein folding but also promotes *Il6* transcription by XBPs binding to the *Il6* promoter in endotoxin-activated macrophages [43]. We sought to investigate if this mechanism holds true for MCs, another important innate immune cell, and particularly focused on *Ship1*-deficient BMMCs. These cells are hyperactive and produce high amounts of pro-inflammatory cytokines in response to Fc ϵ RI crosslinking [44]. A dependence of IL-6 production should be investigated using the IRE1 α inhibitor KIRA6 [18]. Indeed, preliminary experiments showed that pretreatment with KIRA6 causes attenuation of Ag-triggered IL-6 production/secretion (data not shown). As a matter of routine, we used the same cellular supernatants to also measure for the presence of the lysosomal enzyme β -hexosaminidase, which, in contrast to IL-6, is released within minutes after Fc ϵ RI activation. Unexpectedly, however, a severe reduction of secreted β -hexosaminidase was found in the cellular supernatant of KIRA6-pretreated *Ship1*^{-/-} BMMCs (data not shown). Kinetically/mechanistically, no obvious reason could explain why this immediate β -hexosaminidase-releasing degranulation process should depend on the activity of the ER stress sensor IRE1 α or the transcription factor XBPs. Hence, we set out to analyze whether KIRA6 affects MC activation in an off-target manner.

We pretreated *Ship1*^{+/+} and *Ship1*^{-/-} BMMCs with DMSO (vehicle) or rising concentrations of KIRA6 (0.03–1 μM), stimulated with Ag (DNP-HSA), and determined the release of

β -hexosaminidase. In agreement with previous data, the release of β -hexosaminidase was considerably stronger from *Ship1*^{-/-} compared with *Ship1*^{+/+} BMMCs [25, 26]. Intriguingly, KIRA6 inhibited Ag-triggered degranulation in *Ship1*^{+/+} BMMCs starting at a concentration of 0.03 μM , whereas in *Ship1*^{-/-} BMMCs an approximately 30x higher concentration of KIRA6 (1 μM) was necessary to obtain a comparable level of inhibition (Figure 1A).

To support our findings, we additionally made use of the LAMP1 assay for interrogating Ag-triggered secretion. LAMP1, a.k.a. CD107a, is expressed in the membrane of secretory lysosomes and is thus extracellularly not detectable in resting MCs by fluorescently labeled anti-LAMP1 antibodies. Upon Ag stimulation, vesicle membranes fuse with the plasma membrane and hence allow for detection of LAMP1 using flow cytometry. As shown in Figure 1B, results comparable to the β -hexosaminidase assay were obtained in *Ship1*^{+/+} and *Ship1*^{-/-} BMMCs. *Ship1*^{+/+} BMMCs once again were considerably more sensitive to KIRA6 pretreatment compared with *Ship1*^{-/-} cells.

Next, we investigated the effect of KIRA6 on Ag-induced pro-inflammatory cytokine production in *Ship1*^{+/+} and *Ship1*^{-/-} BMMCs by measuring secreted IL-6 and TNF. As expected, *Ship1*^{-/-} BMMCs upon Ag stimulation produced dramatically more cytokines than *Ship1*^{+/+} BMMCs [45, 44] (Figure 1C,D). Again, KIRA6-mediated inhibition was more efficient in *Ship1*^{+/+} compared with *Ship1*^{-/-} BMMCs (Figure 1C,D). Intriguingly, in *Ship1*^{-/-} BMMCs low concentrations of KIRA6 first resulted in an increase in cytokine production before a significant reduction occurred with 1 μM KIRA6 (Figure 1C,D). As mentioned above, the immediate response of degranulation kinetically does not coincide with an ER stress-induced activation of the UPR sensor IRE1 α , hence ruling out KIRA6-mediated inhibition of IRE1 α as a molecular reason for suppression of degranulation. The process of cytokine production, however, could fit to activation of IRE1 α and resulting *Xbp1* splicing, as it has been demonstrated in LPS-stimulated macrophages [43]. Therefore, we measured *Xbp1* splicing in Ag- and stem cell factor (SCF)-triggered *Ship1*^{-/-} BMMCs and the potential inhibitory effect of KIRA6. As shown in Figure 1E, virtually no induction of *Xbp1* splicing, and thus, no effect of KIRA6 was measurable. However, successful Ag and SCF co-stimulation and inhibition by KIRA6 were verified by measuring production of *Il6* mRNA (Figure 1F). To finally rule out the participation of IRE1 α in Ag-triggered degranulation, we compared the effect of KIRA6 pretreatment with the efficiency of the more recent and selective KIRA8 [46]. Indeed, compared with KIRA6, KIRA8 did not suppress β -hexosaminidase release even at 1 μM (Figure 1G). Nanomolar efficacy of KIRA8 was verified in HMC-1.2 MC leukemia cells stressed with tunicamycin causing strong *XBPI* splicing (Figure S1). In conclusion, the IRE1 α inhibitor KIRA6 suppresses immediate and sustained Ag-triggered MC activation in an IRE1 α -independent manner.

3.2 | Early Ag-triggered Signaling Processes Are Sensitive to KIRA6

Degranulation of MCs can also be triggered by a combination of the Ca²⁺ ionophore A23187 and the PKC activator PMA [8].

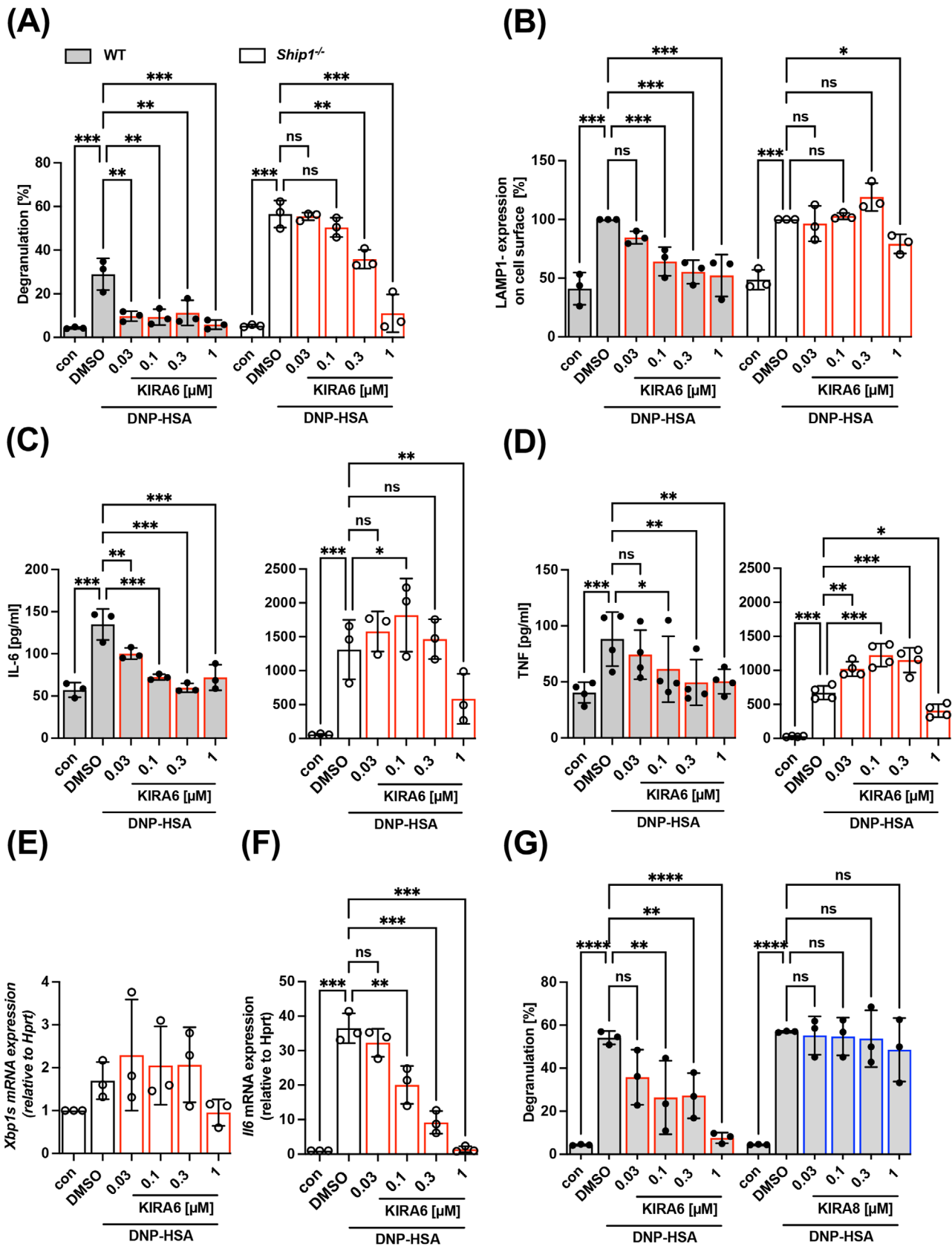


FIGURE 1 | KIRA6 inhibits degranulation and cytokine production of WT and *Ship1*^{-/-} BMMCs. IgE pre-loaded WT (gray bars) or *Ship1*^{-/-} BMMCs (white bars) were incubated with solvent control DMSO or the indicated KIRA6 (red line) or KIRA8 (blue line) concentrations for 1 h followed by Ag-stimulation with 20 ng/mL DNP-HSA (A–D, G) or combined stimulation with 100 ng/mL SCF (E, F). (A) Degranulation was determined by calculating the enzymatic activity of released β -hexosaminidase in relation to total β -hexosaminidase activity after stimulation of WT and *Ship1*^{-/-} cells with DNP-HSA for 30 min ($n = 3$). (B) Cell surface localized LAMP1 was detected by flow cytometry in unstimulated and DNP-HSA-stimulated (5 min) WT and

Comparison of the KIRA6 effect on degranulation of BMMCs in response to Ag versus the combination of A23187+PMA was supposed to allow to determine if the target of KIRA6 is localized up- or downstream of the Ca^{2+} mobilization step mandatory for degranulation. In contrast to Ag, A23187 + PMA-induced degranulation of WT BMMCs was not suppressed by KIRA6 (Figure 2A). This suggested that KIRA6 inhibits an immediate step in Fc ϵ RI-induced signal transduction, which precedes Ca^{2+} mobilization and/or PKC activation. This might be the activation of PLC γ , which hydrolyzes PI4,5P $_2$ to yield IP $_3$ and DAG responsible for Ca^{2+} release from the ER and PKC activation at the plasma membrane, respectively. Confirming this assumption, KIRA6 dose-dependently and efficiently suppressed the activating phosphorylation of PLC γ 1 at Tyr783 in response to Ag stimulation (Figure 2B). In agreement, KIRA6 repressed Ag-triggered Ca^{2+} mobilization in a dose-dependent fashion (Figure 2C; Figure S2). In conclusion, KIRA6, put on the market as an IRE1 α inhibitor, is capable of effectively suppressing Ag-triggered MC signaling and effector responses apparently by inhibiting an additional target protein (e.g., a Fc ϵ RI-associated kinase).

In previous work, we found that *Lyn* deficiency results in a comparable reduction of PLC γ phosphorylation and Ca^{2+} mobilization as currently observed for KIRA6 action [12]. Indeed, analysis of total substrate Tyr phosphorylation revealed almost its complete inhibition by KIRA6 pretreatment in *Ship1*^{+/+} and *Ship1*^{-/-} BMMCs already as early as 1 min after the addition of Ag (Figure 2D; Figure S3A), again hinting at LYN as a KIRA6 target. A further characteristic of Ag-stimulated *Lyn*^{-/-} BMMCs was the delayed and weakened phosphorylation of ERK1/2 [12], which was also found in KIRA6-treated *Ship1*^{+/+} and *Ship1*^{-/-} BMMCs, in addition to a repression of MEK1/2, JNK, and PKB phosphorylation (Figure 2E; Figure S3B). In conclusion, KIRA6 suppresses immediate early Ag-triggered signaling processes, a pattern which is suggestive of the SFK LYN being the/an additional target of KIRA6.

3.3 | Pharmacological Inhibition of LYN by KIRA6

A specific substrate of LYN in Ag-triggered BMMCs is the lipid phosphatase SHIP1, which attenuates PI3K signaling and IgE-mediated effector functions [12, 11]. In accordance with LYN being a potential target of KIRA6, pretreatment of BMMCs with KIRA6 resulted in complete abrogation of basal and Ag-induced Tyr phosphorylation of SHIP1 (Figure 3A).

We determined whether KIRA6 can directly bind to recombinant LYN in vitro and calculated the K_d of this interaction. Performing

MST using fluorescently labeled LYN [47], the calculated K_d of KIRA6 was $3.2 \pm 1.2 \mu\text{M}$ (Figure 3B). Moreover, the interaction between LYN and KIRA6 was verified by means of nanodifferential scanning fluorimetry (nanoDSF; a label-free thermal-shift assay technique) to study protein denaturation as a function of temperature [47], which proved a distinct change in the thermal unfolding of recombinant LYN ($\Delta T_m = -3.1^\circ\text{C}$) in the presence of KIRA6 (Figure S4A). Following this, we performed an in vitro kinase assay using immunoprecipitated LYN from BMMC lysates and a GST fusion protein containing the full-length LYN substrate SH3P7 as the substrate [27]. Indeed, we could show that KIRA6 inhibits LYN with an IC_{50} of approximately 300 nM (Figure 1C,D; Figure S4C), illustrating that measurement of direct binding of KIRA6 to recombinant LYN protein using MST correlates qualitatively with in vitro analysis (IVKA).

Being now confident that KIRA6 is a LYN inhibitor in the sub-micromolar range, we compared its efficiency with the potent SFK inhibitor, Saracatinib (AZD-0530), which has been shown in cell-free assays to inhibit LYN with an IC_{50} of 5 nM [48]. However, in different cellular assays, Saracatinib was used at concentrations between 1 and 10 μM [49, 50, 51]. Analysis of Ag-triggered substrate Tyr phosphorylation by Western blotting as well as measurement of β -hexosaminidase release revealed a considerable difference in effectiveness between KIRA6 and Saracatinib, with KIRA6 being more efficient by a factor of approximately 30 (Figure 3E,F). In conclusion, our findings indicate that KIRA6 binds to and inhibits the SFK LYN in the sub-micromolar range, effectively suppressing Ag-triggered MC activation.

3.4 | Use of *Lyn*-deficient BMMCs Corroborates LYN Inhibition by KIRA6 and Suggests Additional Suppression of FYN at Higher Concentrations

Given that KIRA6 is a potent LYN inhibitor, it should not suppress Ag-induced degranulation or cytokine production in LYN-deficient MCs, at least not at low nanomolar concentrations effective in WT cells. Therefore, we generated *Lyn*^{-/-} BMMCs and compared their Ag-triggered effector and signaling functions to WT (*Lyn*^{+/+}) BMMCs in the presence or absence of KIRA6. First, we analyzed Ag-induced degranulation (β -hexosaminidase release) in the presence of increasing concentrations of KIRA6. While KIRA6 treatment of *Lyn*^{+/+} cells caused progressive attenuation of degranulation between 0.03 and 0.3 μM of KIRA6, no such effect was observed in *Lyn*^{-/-} BMMCs (Figure 4A). At 1 μM of KIRA6, however, complete suppression of degranulation was observed in both *Lyn*^{+/+} and *Lyn*^{-/-} cells, suggesting that at this concentration one or more additional KIRA6-sensitive kinases,

Ship1^{-/-} BMMCs ($n = 3$). (C) Secreted IL-6 ($n = 3$) and (D) TNF ($n = 4$) were measured by ELISA assays after 4 h of DNP-HSA stimulation from supernatants of stimulated and unstimulated WT and *Ship1*^{-/-} cells. (E) *Xbp1s* and (F) *Il6* mRNA expression were detected by RT-qPCR after combined stimulation with 100 ng/mL SCF 5 min prior to the addition of DNP-HSA for 4 h in *Ship1*^{-/-} BMMCs (both $n = 3$). *Hprt* served as a housekeeping gene to which mRNA expression of genes of interest was normalized. (G) WT BMMCs were pre-incubated with KIRA6 or KIRA8 followed by DNP-HSA stimulation for 30 min and the percentage of released β -hexosaminidase was calculated ($n = 3$). The data presented are derived from 3 (A–F) or 4 (D) independent experiments, each comprising three technical replicates for all indicated samples. Data are shown as mean \pm SD. Symbols indicate individual values of biological replicates. (A), (B), and (G) two-way ANOVA followed by Sidak's multiple comparisons test. (C–F) RM one-way ANOVA followed the Dunnett test to correct for multiple comparisons. * $p < 0.05$, ** $p < 0.01$, *** $p < 0.001$, **** $p < 0.0001$; ns indicates nonsignificance.

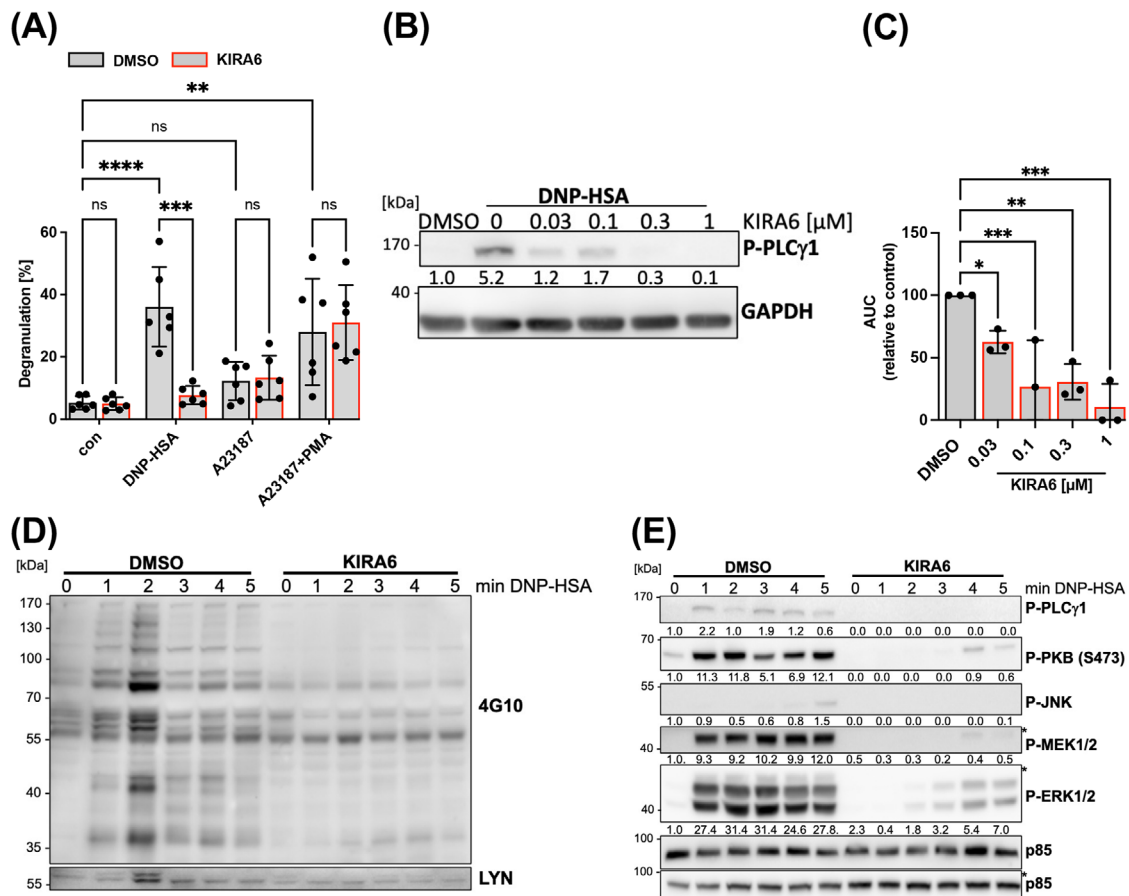


FIGURE 2 | KIRA6 inhibits FcεRI-dependent signaling in WT BMMCs. IgE-preloaded WT BMMC (gray bars) was incubated with the solvent control DMSO or the indicated KIRA6 (red line) concentrations for 1 h followed by incubation with the indicated stimuli. (A) Degranulation was induced by DNP-HSA (20 ng/mL), A23187 (100 ng/mL), or the combination of A23187 (100 ng/mL) and PMA (100 ng/mL) for 30 min, and the percentage of released β-hexosaminidase in relation to total β-hexosaminidase was calculated ($n = 6$). (B) IgE-preloaded WT BMMCs were starved overnight, incubated with indicated KIRA6 concentrations or DMSO for 1 h and subsequently stimulated with DNP-HSA (20 ng/mL) for 1 min. PLCγ1 phosphorylation at Tyr783 was assessed by Western blot using a phospho-specific antibody. GAPDH served as a loading control ($n = 3$). (C) Ca²⁺ mobilization was induced by SCF and DNP-HSA co-stimulation and determined by the ratio of the Ca²⁺-bound /Ca²⁺-unbound using the Ca²⁺-sensitive fluorophores Fluo-3 and FuraRed. The graph shows the normalized comparison of the area under the curve (AUC) values representing total Ca²⁺ mobilized within 4 min after stimulation ($n = 3$). (D) Representative Western blot showing global tyrosine phosphorylation after 20 ng/mL DNP-HSA stimulation at the indicated time points using 4G10 antibodies. LYN was detected on the same membrane using an anti-LYN antibody. LYN expression served as loading control ($n = 3$). (E) Representative Western blot showing DNP-HSA-induced phosphorylation of PLCγ1, PKB, JNK, MEK1/2, and ERK1/2 detected by Western blot using phospho-specific antibodies. p85 served as a loading control ($n = 3$). (B, E) Numbers indicate mean values obtained from densitometry analyses. (A, C) The data presented are derived from three independent experiments, each comprising three technical replicates for all indicated samples. (B, D, E) The data show representative Western blots from three independent experiments for all indicated samples. Data are shown as mean ± SD. Symbols indicate individual values of biological replicates. (A) Two-way ANOVA followed by Sidak multiple comparisons test. (B, C) RM one-way ANOVA followed by Dunnett's test to correct for multiple comparison. * $p < 0.05$, ** $p < 0.01$, *** $p < 0.001$; ns indicates nonsignificance.

which are positively regulating MC degranulation, are inhibited, with the SFK FYN being a meaningful candidate [52]. We further analyzed the effect of KIRA6 on the Ag-triggered production of IL-6 and TNF in *Lyn*^{+/+} and *Lyn*^{-/-} BMMCs. As expected, *Lyn*^{-/-} BMMCs, compared with *Lyn*^{+/+} BMMCs, produced considerably higher amounts of proinflammatory cytokines (Figure 4B,C) [12]. As observed for degranulation, a comparable pattern could be demonstrated with respect to IL-6 (Figure 4B) and TNF production (Figure 4C) in KIRA6-pretreated (0.03–0.3 μM) *Lyn*^{+/+} and *Lyn*^{-/-} BMMCs. Unexpectedly, secretory responses in LYN-deficient BMMCs were even promoted by KIRA6 in the range of 0.03–0.3 μM (Figure 4A–C), which might depend on differential sensitivity for KIRA6 of the different SFKs expressed in MCs

(Figure S6C) as well as respective differences between *Lyn*^{+/+} and *Lyn*^{-/-} BMMCs. Nevertheless, our observations using *Lyn*^{-/-} BMMCs clearly corroborate the LYN-specific action of KIRA6 at sub-micromolar concentrations.

The further analysis of Ag-triggered signaling events in *Lyn*^{+/+} and *Lyn*^{-/-} BMMCs in the absence or presence of KIRA6 completed the picture (Figure 4D). Ag-induced phosphorylation of PLCγ1, PKB, ERK1/2, and IκBα was markedly reduced in the absence of LYN [12], and the remaining phosphorylations in *Lyn*^{-/-} BMMCs were suppressed to background levels by 1 μM KIRA6 (Figure 4D), again suggesting the presence of an additional KIRA6 target.

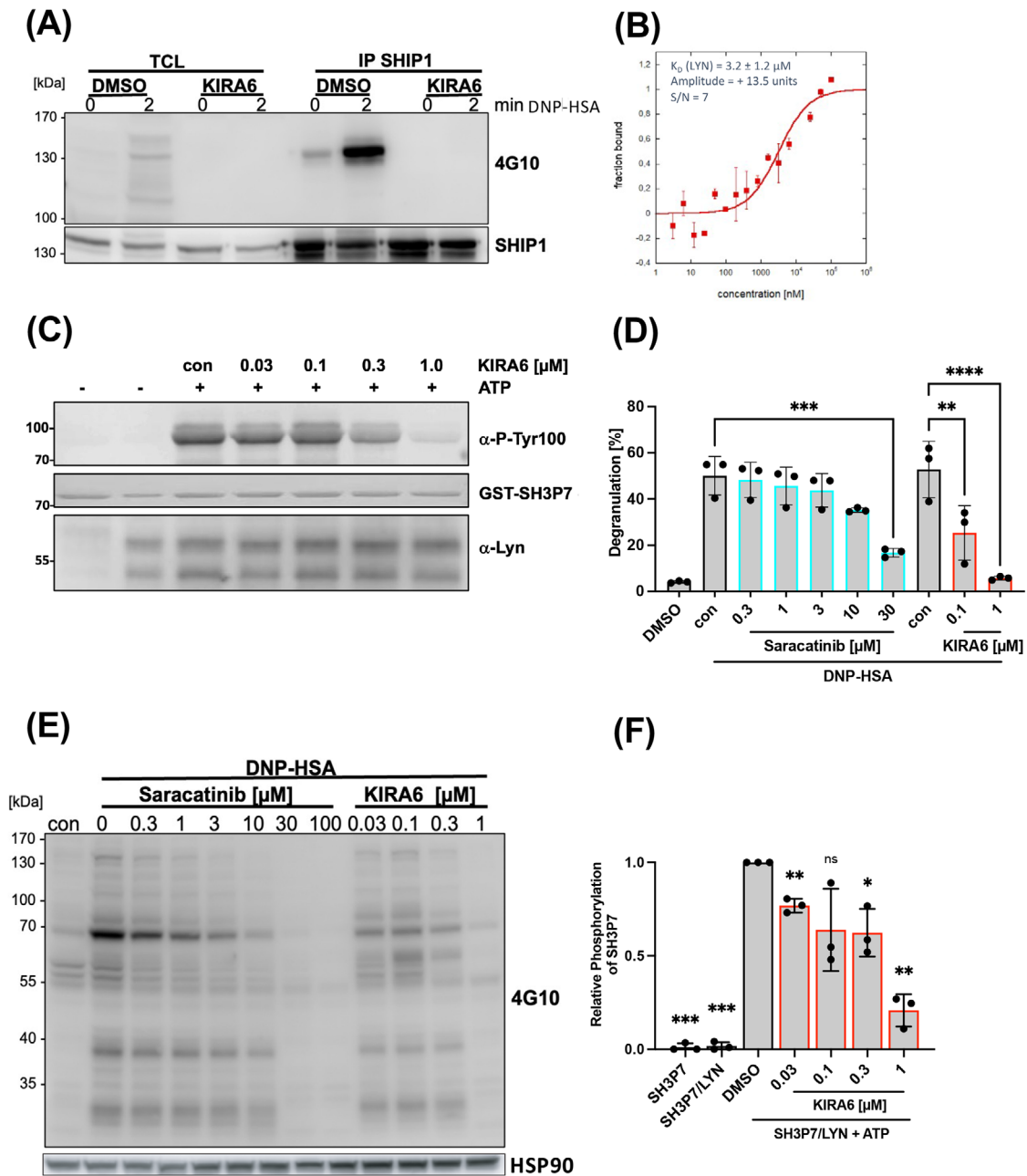


FIGURE 3 | KIRA6 efficiently inhibits LYN kinase activity. (A) IgE-sensitized WT BMMCs were pre-incubated with 1 μM KIRA6 for 60 min before cells were left unstimulated or stimulated with 20 ng/mL DNP-HSA for 2 min. SHIP1 was immunoprecipitated from cell lysates and tyrosine phosphorylation of SHIP1 was detected on WB using 4G10 antibodies. A comparable amount of SHIP1 in the TCL and the precipitates was confirmed by staining with anti-SHIP1 antibody ($n = 3$). (B) Concentration-dependent ligand binding of KIRA6 to LYN was evaluated with MicroScale thermophoresis (MST) to calculate the K_D . Error bars represent the standard deviation of two independent experiments in (two technical repeats each) ($n = 2$). (C) LYN kinase activity was determined in vitro by the detection of the phosphorylated LYN substrate GST-SH3P7 using a pTyr-specific antibody. The substrate was incubated with precipitated LYN and the reaction was performed in the presence of 200 mM ATP for 30 min at RT. Ponceau S was used to stain recombinant GST-SH3P7 on the WB membrane and an anti-LYN antibody to show comparable amounts of LYN in each sample. (D) Relative SH3P7 phosphorylation of independently performed LYN kinase assays was quantified in comparison to the positive control (DMSO) using the solvent DMSO with LYN and SH3P7 in the presence of ATP. Relative phosphorylation intensity was determined by densitometry analysis ($n = 3$). (E, F) IgE-sensitized WT BMMCs were incubated with indicated concentrations of Saracatinib and KIRA6 for 60 min before DNP-HSA stimulation. (E) Global tyrosine phosphorylation following DNP-HSA stimulation and KIRA6 or Saracatinib (Sara) pretreatment ($n = 3$). (F) The influence of Sara and KIRA6 on DNP-HSA-induced degranulation was calculated by the percentage of released in relation to total β -hexosaminidase ($n = 3$). (A, C–E) The data show representative Western blots of three independent experiments for all indicated samples. (B) The error bars represent the standard deviation of two independent experiments, each comprising two technical repeats. (F) The data presented are derived from three independent experiments, each comprising three technical replicates for all indicated samples. (D, F) Data are shown as mean \pm SD. Symbols indicate individual values of biological replicates. (D) One sample t -test in comparison to the positive control (DMSO, LYN, SH3P7, ATP). (F) was analyzed by ordinary one-way ANOVA followed by Sidak's multiple comparison test. * $p < 0.05$, ** $p < 0.01$, *** $p < 0.001$, **** $p < 0.0001$; ns indicates nonsignificance.

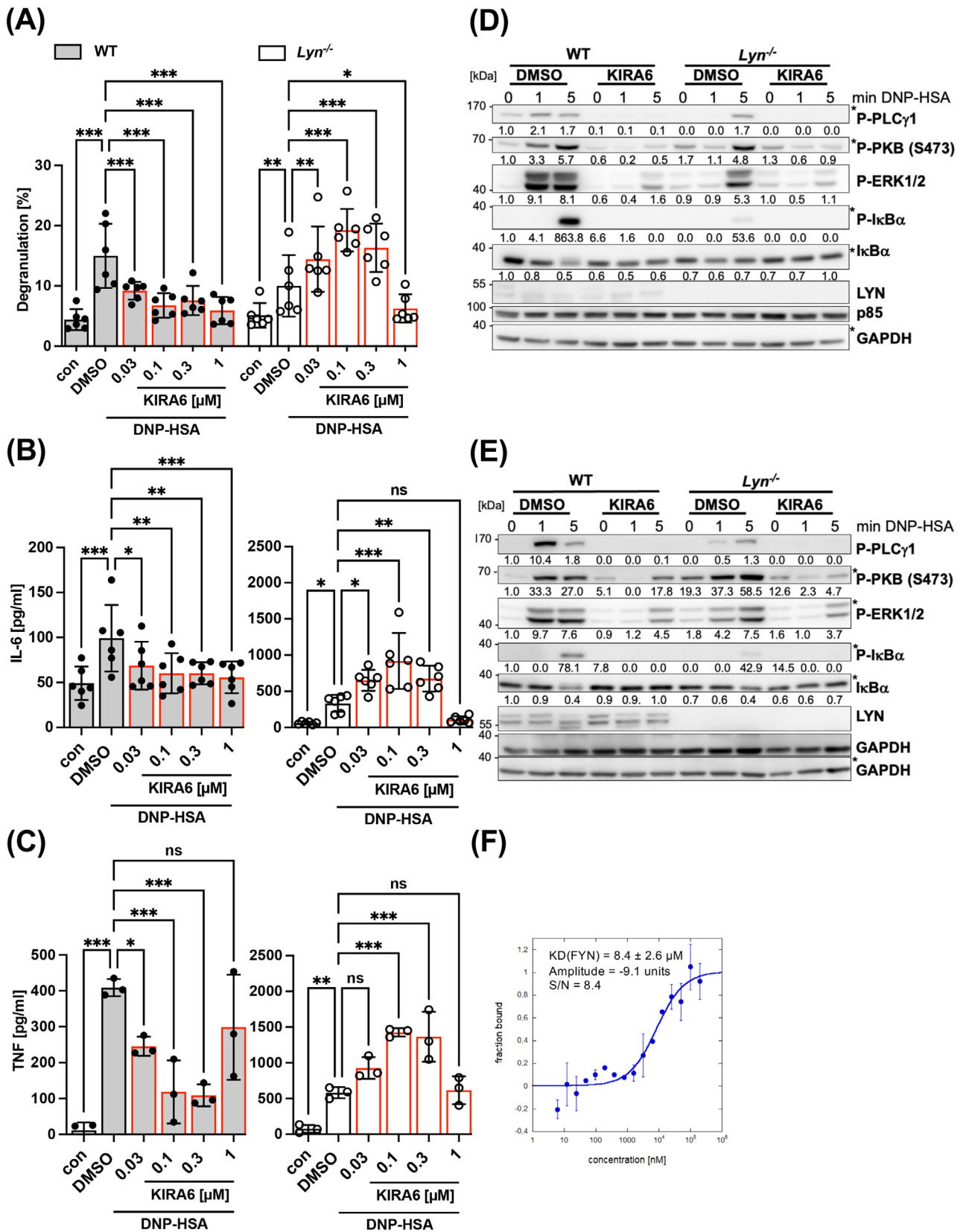


FIGURE 4 | KIRA6 additionally affects FYN activation. IgE-preloaded WT BMMC (gray bars) or *Lyn*^{-/-} BMMCs (white bars) were incubated with the solvent control DMSO or the indicated KIRA6 (red line) concentrations for 1 h followed by antigen stimulation with 20 ng/mL DNP-HSA. (A) Degranulation was calculated by the percentage of released in relation to total β -hexosaminidase after stimulation with DNP-HSA for 30 min ($n = 5$). (B) Released IL-6 and (C) TNF were measured by ELISA assays after KIRA6 pretreatment followed by DNP-HSA stimulation for 4 h (both $n = 6$). (D) 20 ng/mL DNP-HSA or (E) 200 ng/mL DNP-HSA were used to stimulate WT or *Lyn*^{-/-} BMMCs for the indicated time points to induce Fc ϵ RI-dependent phosphorylation of PLC γ 1, PKB, ERK1/2, and I κ B α shown on WB using phospho-specific antibodies. P85 and GAPDH served as loading controls.

Intriguingly, LYN is capable of both positively and negatively regulating FcεRI-mediated MC activation with higher concentrations of crosslinking stimulus shifting the balance to inhibitory functions [53]. Hence, particularly PKB is strongly phosphorylated in *Lyn*^{-/-} BMMCs in response to high Ag concentrations [53, 12]. Since PKB phosphorylation is dependent on PI3K, the activation of which has been proven to require FYN activity [52], we made use of this signaling system to interrogate the potential susceptibility of FYN for inhibition by KIRA6. Increasing the antigen stimulus (DNP-HSA) from 20 ng/mL (Figure 4D) to 200 ng/mL (Figure 4E) resulted in the expected enhanced phosphorylation of PKB in *Lyn*^{-/-} compared with *Lyn*^{+/+} BMMCs. This increased, FYN-dependent PKB phosphorylation [52] could be abrogated by KIRA6 almost completely (Figure 4E). Moreover, direct binding of KIRA6 to recombinant FYN was analyzed using MST and a K_d of 8.4 ± 2.6 μM was determined (Figure 4F). The performance of nanoDSF proved interaction between FYN and KIRA6 as well (Figure S4B). Hence, these data strongly suggested that FYN can be inhibited by 1 μM KIRA6. In conclusion, our data reveal that KIRA6 is a potent LYN inhibitor and, additionally, a reasonable FYN inhibitor, enabling KIRA6 by this combined action to efficiently suppress proinflammatory FcεRI-mediated MC activation.

To additionally exclude that the need for higher KIRA6 concentrations to inhibit activation of *Lyn*^{-/-} BMMCs is due to a potential general KIRA6 insensitivity of these cells, we analyzed the effect of KIRA6 on *Lyn*^{+/+} and *Lyn*^{-/-} BMMCs treated with the LYN-independent ER stressor thapsigargin. Thapsigargin inhibits the SERCA located in the ER membrane resulting in an immediate increase of the cytosolic Ca²⁺ concentration, which causes IgE-independent MC activation [54]. *Lyn*^{+/+} and *Lyn*^{-/-} BMMCs were pretreated with increasing concentrations of KIRA6, subsequently treated with thapsigargin, and production of *Xbp1s* and *Il6* mRNA (Figure 5A–D) as well as IL-6 and TNF protein (Figure S5E,F) were measured. Both cell types produced comparable amounts of *Xbp1s* and *Il6* mRNA as well as IL-6 and TNF protein, and 1 μM KIRA6 was needed for significant reduction of the different MC responses. These data indicate that *Lyn*^{+/+} and *Lyn*^{-/-} BMMCs, in principle, are comparably sensitive to KIRA6 when addressing an LYN-independent signaling process.

3.5 | KIRA6 suppresses MC Activation in an Ex Vivo Model and in human MCs

To extend our study to IgE-mediated MC activation in a tissue-type situation, we made use of a model of PCLS, interrogating the inhibitory effect of KIRA6 on allergen-induced bronchoconstriction in rat lung slices. Due to their intact microanatomy, PCLS

allow for the investigation of whole-lung functions in a reproducible manner [55]. PCLS were pretreated with serum from rats sensitized with ovalbumin, and allergen-induced bronchoconstriction was measured in the absence or presence of increasing concentrations of KIRA6. Allergen-induced bronchoconstriction was significantly suppressed by 1 μM KIRA6 (Figure 5A). The need for a higher drug concentration compared with experiments with BMMCs is most likely due to the reduced permeability of the tissue preparation. As a control, methacholine-induced bronchoconstriction, which is mediated by the muscarinic acetylcholine receptor, was not affected by preincubation with KIRA6 (Figure 6SA).

Next, we aimed to analyze the inhibitory action of KIRA6 on human MCs. First, we used the SCF-dependent human MC line ROSA^{KIT WT} as a model system. IgE-preloaded ROSA^{KIT WT} MCs were activated by anti-IgE-triggered FcεRI crosslinking in the absence or presence of KIRA6, and *IL8* mRNA expression was measured by RT-qPCR. Significant suppression was already measurable using 0.3 μM KIRA6 (Figure 5B). Finally, not to only rely on a human MC cell line, we utilized IgE-sensitized CBMCs, activated them using anti-IgE antibodies, and measured the release of the protease tryptase. Again, KIRA6 (1 μM) was able to significantly inhibit the degranulation process (Figure 5C). In conclusion, KIRA6 treatment was able to inhibit LYN/SFK-dependent MC activation not only in murine BMMCs but also in the *ex vivo* model of bronchoconstriction in PCLS as well as in different human MC models in response to Ag/IgE-mediated activation.

3.6 | Molecular Modeling Reveals Preferred KIRA6 Interaction With Inactive SFKs

Since our research indicated a strong interaction of KIRA6 with three tyrosine kinases of prominent importance for MC activation (LYN and FYN [this work], and KIT [16]) as well as their inhibition, we aimed in a final step to provide atomistic level data for these interactions. We modeled the binding of KIRA6 to both an active and an inactive conformation of the three kinases LYN, FYN, and KIT. The main factor for discriminating the functional, active state of kinases like FYN, LYN, or KIT from the inactive state has traditionally been the position of a conserved DFG (or, rarely, D[LWY]G) motif in its activation loop [56]. While most inhibitors bind to the active (DFG-in) state, so-called type-II inhibitors bind to a distinct DFG-out conformation and occupy an additional hydrophobic pocket [56, 57]. KIRA6 was docked on both DFG-in and DFG-out conformations of FYN, LYN, and KIT (please see the Methods section for more information on the modeling of these conformations). After performing MD

Phosphorylation signals detected on the same membrane are marked with an asterisk. Numbers indicate mean values obtained from densitometry analyses (both $n = 3$). (F) Concentration-dependent ligand binding of KIRA6 to FYN was evaluated with MicroScale Thermophoresis (MST) to calculate the K_D . Error bars represent the standard deviation of 2 independent experiments in (two technical repeats each) ($n = 2$). The data presented are derived from 6 (A) or 3 (B, C) independent experiments, each comprising three technical replicates for all indicated samples. (D, E) The data show representative Western blots of three independent experiments for all indicated samples. (F) The error bars represent the standard deviation of two independent experiments, each comprising two technical repeats. (A–C) Data are shown as mean \pm SD. Symbols indicate individual values of biological replicates. (A) Two-way ANOVA followed by Dunnett's multiple comparisons test. (B, C) RM one-way ANOVA followed by Dunnett's test to correct for multiple comparison. * $p < 0.05$, ** $p < 0.01$, *** $p < 0.001$, **** $p < 0.0001$; ns indicates nonsignificance.

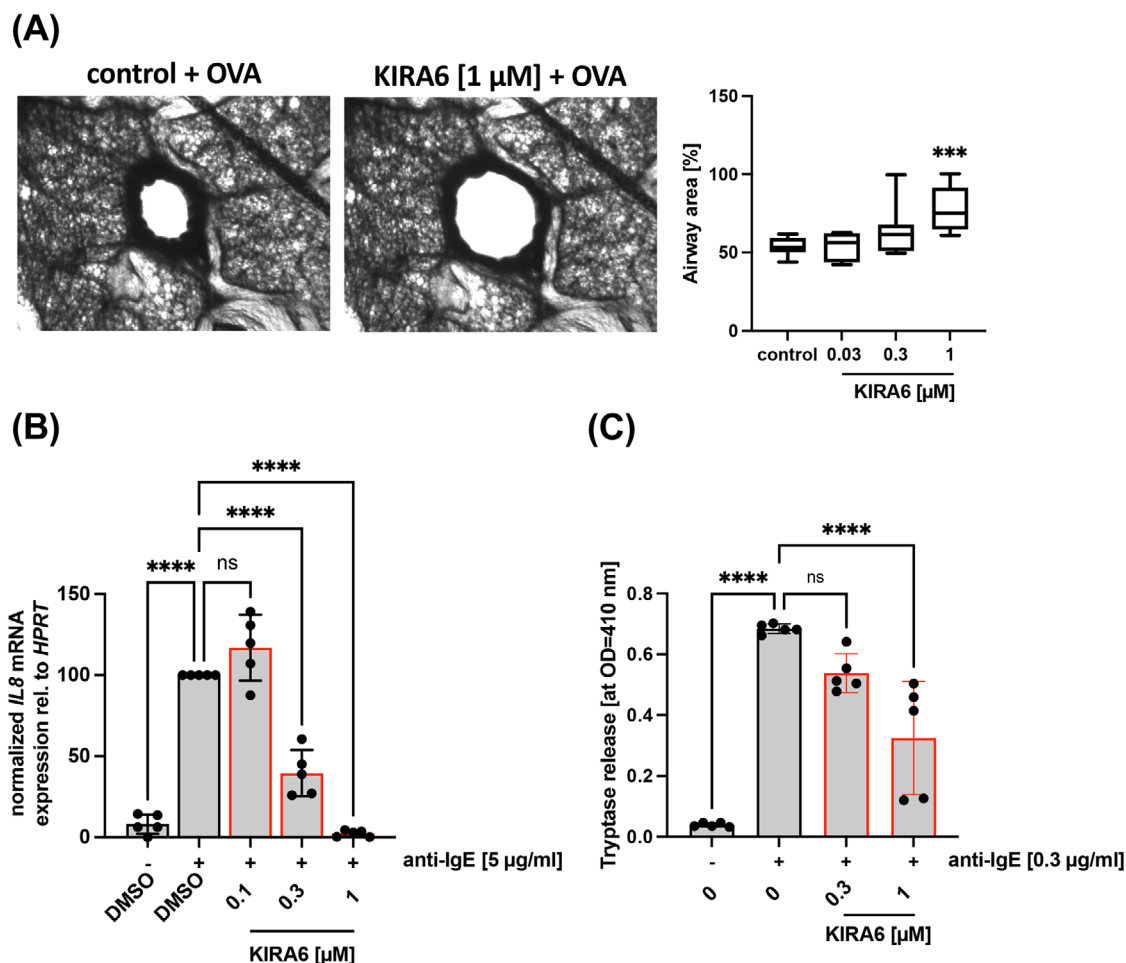


FIGURE 5 | KIRA6 inhibits mast cell function in ex vivo and different human in vitro model systems. (A) Airway contractions to ovalbumin in rat precision-cut lung slices. IgE-sensitized rat precision-cut lung slices were incubated with the solvent control DMSO or the indicated KIRA6 concentration for 5 min prior to challenge with OVA (10 μ g/mL) for 15 min and the degree of bronchoconstriction was determined by evaluation of airway area. The images show airway contraction after preincubation with the solvent control DMSO (left) or 1 μ M KIRA6 (right) and challenge with OVA. The graph shows the response of airway contractions in the presence of the solvent DMSO and the depicted KIRA6 concentration. Contractions are expressed as the decrease of airway area (%) compared with the initial airway area ($n = 10$). (B) IL-4- and IgE-primed ROSA^{KIT WT} cells were pretreated with DMSO or KIRA6 for 1 h and subsequently stimulated or not with 5 μ g/mL α -IgE for 60 min. *IL8* expression was measured by RT-qPCR. *HPRT* served as housekeeping gene to which *IL8* expression was normalized to ($n = 5$). (C) IgE-sensitized CBMCs were pretreated with DMSO or indicated KIRA6 concentration and stimulated with 5 μ g/mL α -IgE for 30 min. Degranulation was evaluated by determining the release of tryptase by an enzymatic assay ($n = 5$). (A) 10 Precision-cut lung slices (samples) were used for each of the four data points to determine the airway area. (B, C) The data presented are derived from five independent experiments, each comprising three technical replicates for all indicated samples. (A–C) Data are shown as mean \pm SD. Symbols indicate individual values of biological replicates. (A–C) ordinary one-way ANOVA followed by Dunnett's test to correct for multiple comparison. * $p < 0.05$, ** $p < 0.01$, *** $p < 0.001$, **** $p < 0.0001$, ns indicates non significance.

simulations to relax the structure and MM GBSA calculations (see methods for details) to estimate the binding affinity, it turned out that KIRA6 has a preference to bind the inactive conformation of the three kinases with a slight preference for KIT and LYN kinases in comparison to FYN (see Table 1).

Specifically, we noticed that while the ligand is nearly fully enclosed in the inactive conformation (Figure 6B,D), significant parts of the ligand are solvent-exposed in the active conformation (see, for example, the trifluoromethyl-phenyl moiety in Figure 6A,C). The trifluoromethyl-phenyl moiety can make use of the additional pocket that is opened by the DFG-out conformation in the inactive state. In particular, there is an additional hydrogen bond between LYN and KIRA6 in the inactive (ASP385, GLU320,

MET322) conformation versus the active (2 \times MET322). These factors can explain the difference in docking score between the active (–6.5) and inactive (–14.4) states in KIRA6 binding to LYN.

4 | Discussion

In the present report, we demonstrate that the IRE1 α inhibitor KIRA6 acts as a very effective inhibitor for the SFK LYN in the nanomolar range, with LYN being one of the main activating and regulatory Tyr kinases in the context of Fc ϵ RI signal transduction in MCs. This was demonstrated, amongst others, by the KIRA6-mediated inhibition of LYN-dependent processes including Ag-induced substrate Tyr phosphorylation, Ca²⁺ mobilization, and

TABLE 1 | Energetics of the last 100 ns of the converged MD trajectories.

Source	ID	Protein	State	ΔH / kcal mol ⁻¹	ΔG / kcal mol ⁻¹	Glide SP docking score*
Modeler	---	LYN	Inactive/DFG-out	-60.6 ± 0.1	-49.4 ± 3	-14.4
Modeler	---	FYN	Inactive/DFG-out	-57 ± 0.1	-33.5 ± 4.4	-12.7
XRAY	6MOB	KIT	Inactive/DFG-out	-67.2 ± 0.1	-58.5 ± 3.2	-15.0
XRAY	2DQ7	FYN	Active/DFG-in	-26.5 ± 0.2	4.9 ± -5.1	-6.5
XRAY	5XY1	LYN	Active/DFG-in	-34 ± 0.1	1.3 ± 5.7	-4.6
XRAY	1PKG	KIT	Active/DFG-in	-27.1 ± 0.1	-0.6 ± 3.5	-5.5

Note: ΔH and ΔG values, as well as, Glide SP docking scores of KIRA6 docked to LYN, FYN, and KIT are listed.

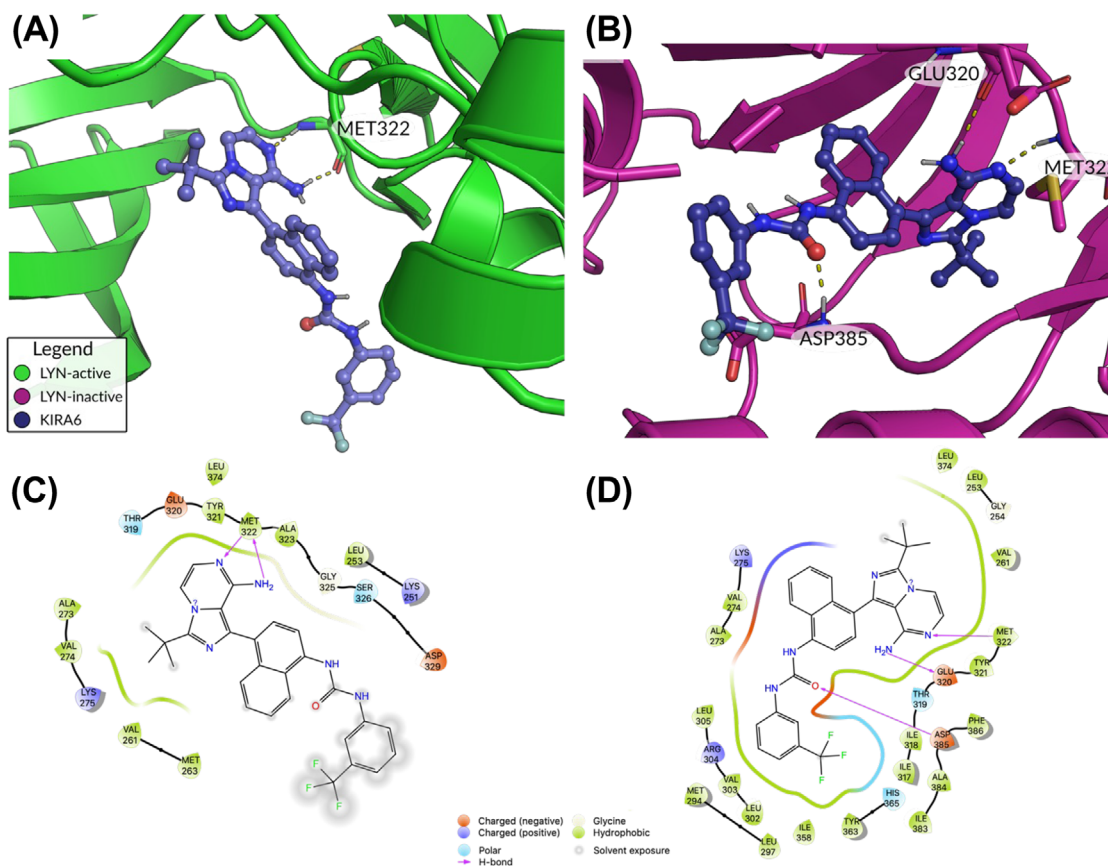


FIGURE 6 | 2D and 3D estimated binding poses of KIRA6 binding to the LYN protein. Predicted binding conformation of KIRA6 in active (DFG-in) (A) and inactive (DFG-out) (B) LYN. Hydrogen bond interactions are visualized with yellow dotted lines. (C, D) 2D representations of the binding poses are shown.

degranulation. These effects are independent of IRE1 α since (1) the concentration required for effective inhibition of IRE1 α is higher than the concentration needed for inhibition of LYN-dependent processes, (2) the more effective and selective IRE1 α inhibitor KIRA8 [46] did not suppress LYN-dependent MC degranulation at a concentration 10-times higher than needed for IRE1 α inhibition, and (3) kinetics of such immediate Ag-triggered processes are, in principle, too fast for a molecular involvement of IRE1 α . Furthermore, MST and nanoDSF measurements and IVKAs convincingly showed that KIRA6 is structurally and functionally interacting with LYN. Moreover, consistent with the functional data, a molecular modeling approach veri-

fied the close interaction of KIRA6 with the catalytic center of LYN in its inactive state. The LYN-dependence of the KIRA6-mediated effects was further confirmed using *Lyn*^{-/-} BMMCs, where KIRA6, at concentrations effective in WT BMMCs, did not suppress Ag-induced degranulation and cytokine production.

Although Ag-triggered effector functions in WT MCs were diminished by KIRA6 in a dose-dependent manner, suppression was only evident at a high concentration of 1 μ M in *Lyn*^{-/-} BMMCs, most likely reflecting inhibition of FYN. LYN appears to have a dominant role in the family of SFKs since it regulates the phosphorylation by the kinase CSK of the C-terminal Tyr residue

of other SFKs, and thus their attenuation. Concurring with the importance of LYN and CSK for MC signaling and regulation of SFKs, our Next Generation Sequencing analysis of BMMCs corroborated the dominant expression of *Lyn* and *Csk* over *Fyn*, *Hck*, and *Src* (Figure S6B). Odom et al. [58] have shown that Tyr phosphorylation of the membrane-spanning CSK-binding protein (CBP; a.k.a. PAG85) is drastically reduced in *Lyn*^{-/-} compared with WT BMMCs, resulting in reduced interaction between CBP and CSK, entailing weaker C-terminal Tyr phosphorylation of FYN and thus its enhanced activity. In agreement, the SFKs LYN, FYN, HCK, and SRC have been demonstrated to associate with CBP [59]. Since our MST, nanoDSF and molecular modeling approaches pointed at KIRA6 being a more efficient inhibitor of LYN than of FYN, the need for a higher concentration of KIRA6 to suppress FcεRI-mediated degranulation and cytokine production in *Lyn*^{-/-} BMMCs goes with such mechanism. This CBP-CSK-driven negative regulation of SFKs was initially described in T-lymphocytes [60] and was mostly accepted to take place in further immune cells. Interestingly however, thoroughly analyzing CBP knockout and knockdown BMMCs, Draberova et al. identified a positive function for CBP as well with respect to Ag-triggered effector mechanisms [61], suggesting a more complex regulation of SFK-mediated MC activation. In this regard, the affinity of LYN's SH2-domain for a phospho-Tyr residue within CBP was found to be distinctly higher than for its phosphorylated C-terminal Tyr508 [62], indicating that CSK-mediated phosphorylation of LYN (and maybe of other SFKs as well) does not automatically result in inactivation of LYN.

Our initial observation that KIRA6 inhibits Ag-triggered MC activation was made in *Ship1*^{-/-} BMMCs, where, compared with wildtype BMMCs, a higher concentration of KIRA6 was necessary for significant suppression of MC effector functions. *Ship1*^{-/-} BMMCs stand out due to their dramatic accumulation of the PI3K-generated signaling phospholipid, PIP₃, and consecutive recruitment/activation of PIP₃-dependent proteins, particularly PKB [63, 64], via their PH-domains. Interestingly, FcεRI-induced PI3K activation demands the functional interaction between the SFK FYN, PI3K, and the adaptor protein GAB2 [52]; the latter translocates to the plasma membrane using its PIP₃-binding PH-domain, potentially organizing an activation-stabilizing/prolonging feed-forward circuit. Hence, SHIP1 deficiency could promote the GAB2-FYN axis and render the cells less dependent on LYN activity. Thus, as observed in our study, *Ship1*^{-/-} BMMCs would be less susceptible to inhibition by low concentrations of KIRA6. In this regard, differences in the LYN/FYN ratio between types of (mast) cells could define susceptibility to inhibition by a pharmaceutical agent derived from KIRA6 as a pharmacophore.

Although LYN deficiency results in enhanced cytokine production upon Ag treatment [52, 11, 12], no increase has been observed in Ag-stimulated WT BMMCs under KIRA6 treatment. Though 1 μM KIRA6 appears to be required to fully inhibit FYN action, suboptimal suppression of FYN at lower concentrations of KIRA6 might already alleviate the potential cytokine-enhancing effect of LYN inhibition by KIRA6, resulting in a reduction of IL-6 and TNF production. Moreover, in addition to LYN and FYN, other SFKs (e.g., HCK and SRC) might also be slightly inhibited, and the composite effect could lead to attenuated cytokine production. In principle, SFKs can be classified into two subfamilies, where HCK

can be regarded as LYN-related, and FYN as well as SRC belong to the SRC-related subfamily [62].

Due to the structural similarities of SFKs, the generation of selective inhibitors for particular kinases seems rather difficult. In addition, MCs express several different SFKs, namely LYN, FYN, SRC, and HCK (Suppl. Figure 6B). Complicating the picture even more, most of them exert important, sometimes opposing functions (exemplified by Hong et al. [65], Parravicini et al. [52], and various publications on the role of LYN [11, 12, 52]). The frequently used inhibitors PP1 and PP2 are called SRC-family selective Tyr kinase inhibitors, which points out that these drugs are nonselective for the specific/individual SFK members. Moreover, the SFK least inhibited by these drugs, showing the highest IC₅₀, appears to be LYN. Another well-known SFK inhibitor, SU6656, inhibits LYN with a fairly low IC₅₀ (approx. 130 nM). However, the respective IC₅₀ for FYN unfortunately is very close (app. 170 nM), making this drug rather useless for a differentiation between LYN- and FYN-mediated functions. Our data reported in this study suggest a considerable difference concerning the concentrations of KIRA6 required for the inhibition of LYN and FYN. This suggests that the structure of KIRA6 as a pharmacophore might be used for the development of novel LYN- and FYN-selective inhibitors.

KIRA6 was developed as a kinase-inhibiting RNase-attenuating molecule [18]. It is a type II inhibitor inhibiting IRE1α phosphorylation in an ATP-competitive manner stabilizing its inactive kinase conformation [18]. Effectivity and selectivity were verified by performing ON-target competition tests, particularly with respect to IRE1α-mediated *XBPI* cleavage in vitro and *XBPI* mRNA splicing in vivo. It was further proven that KIRA6 does not inhibit kinase activity in vitro regarding a panel of Ser/Thr kinases (including ERK2, JNK2, and PKA) [18]. A further study applying kinase photoaffinity labeling combined with mass spectrometry analysis, however, suggested that KIRA6 might be not as selective as initially aimed for with the majority of off-targets not being protein kinases but mostly nucleotide-binding proteins [66, 67]. However, these analyses were performed in cellular lysates using a rather high concentration of labeled KIRA6 (10 μM) and thus it remains to be shown if such concentration can also be reached in living cells or if these proteins also serve as KIRA6 targets in living cells. Obviously, the highest concentration of KIRA6 needed in our study, depending on the MC type studied, was 1 μM, and the comparison of wild-type and LYN-deficient BMMCs clearly showed the necessity of the presence of LYN for a KIRA6 effect in the nanomolar range. Intriguingly, though the MC-relevant kinases attenuated by KIRA6 in our present and former studies [16] are Tyr kinases, our modeling approach indicated that KIRA6 acts as a type II inhibitor as well.

We have analyzed the toxicity of KIRA6 on MC proliferation, metabolic activity, and viability. Wild-type and SHIP1-deficient BMMCs were incubated with various concentrations of KIRA6 for up to 72 h. Importantly, cell viability was not affected by KIRA6 treatment within the first 24 h (Figure S7A,B). However, cytotoxic effects of KIRA6 were observed at concentrations of 1 μM and above after 72 h of exposure (Figure S7C–H). It has been shown, that this concentration was not only sufficient to inhibit IRE1α but also proved cytotoxic to HMC-1.2 cells [68]. Importantly, lower concentrations of KIRA6, which were sufficient to inhibit

the kinases FYN and LYN, did not exhibit cytotoxic effects in BMMCs.

When deciding on the preferable quality of a pharmacological inhibitor in a situation-dependent manner, questions arise like (1) how selective does an inhibitor have to be, and (2) how much promiscuity for substrate proteins can be allowed or even desirable? In chronic lymphocytic leukemia, for instance, LYN has been demonstrated to be essential for the formation of a microenvironment supporting leukemic growth [69], and hence in such a situation, a high selectivity for LYN inhibition would be desirable. On the other hand, in MCs upon IgE- or KIT-mediated activation, LYN represents an important activating signaling element with attenuating functions as well, hence potentially restricting the application of highly selective inhibitors [53, 12, 11]. LYN deficiency results in enhanced Ag-triggered pro-inflammatory cytokine production as well as in increased SCF-induced proliferation. Thus, for MC inhibition in the context of IgE-dependent allergic or KIT-driven neoplastic diseases, co-inhibition of LYN, FYN, and KIT would be an evident advantage.

5 | Data Limitations and Perspectives

Using biochemical, cell biological, and biophysical techniques, combined with homology modeling and molecular dynamics simulations, we could demonstrate that the IRE1 α inhibitor KIRA6 acts as an effective inhibitor of the SFKs LYN and FYN. Thus, KIRA6 was able to efficiently suppress IgE-mediated proinflammatory MC activation. Different types of MCs seemed to show differential sensitivity to KIRA6, with the cellular environment most likely playing a critical role in terms of drug solubility and/or stability. We believe this is the reason, why KIRA6 was unable to reduce antigen-mediated tryptase release in an in vivo study using a direct peritonitis model (Figure S6C). We do not recommend the use of KIRA6 as an MC inhibitor in patients with allergies or other inflammatory diseases involving MCs, since the combined inhibitory activity against SFKs, KIT [16], and the ubiquitous UPR sensor IRE1 α could cause detrimental side effects. Nevertheless, based on our comprehensive analysis of this drug, we suggest that the (sub-) structure of KIRA6 could be used as a pharmacophore to develop novel effective MC stabilizers. However, the required development of novel organic chemicals with subsequent in vitro and in vivo drug testing was beyond the scope of this study.

Author Contributions

Conceptualization: Michael Huber and Thomas Wilhelm. Data curation: Veronika Wunderle, Thomas Wilhelm, Giulia Rosetti, Jonas Goßen, and Michael A. Margreiter. Formal analysis: Veronika Wunderle, Thomas Wilhelm, Michael A. Margreiter, Jonas Goßen, and Thomas Schubert. Funding acquisition: Michael Huber, Boaz Tirosh, Francesca Levi-Schaffer. Investigation: Veronika Wunderle, Thomas Wilhelm, Shatha Boukeileh, Roman Sakurov, Sandro Capellmann, Maike Schwoerer, Nabil Ahmed, Gina Bronneberg, Christian Martin, and Thomas Schubert. Methodology: Giulia Rosetti, Jonas Goßen, Michael A. Margreiter. Project administration: Michael Huber and Thomas Wilhelm. Resources: Michael Huber, Giulia Rosetti, Francesca Levi-Schaffer, Boaz Tirosh, and Michel Arock. Software: Giulia Rosetti, Michael A. Margreiter, and Jonas

Goßen. Supervision: Thomas Wilhelm, Michael Huber, Boaz Tirosh, Francesca Levi-Schaffer, and Giulia Rosetti. Validation: Veronika Wunderle and Thomas Wilhelm; Visualization: Veronika Wunderle, Thomas Wilhelm, and Michael Huber. Writing—original draft: Thomas Wilhelm, Michael Huber, and Veronika Wunderle. Writing review and editing: Thomas Wilhelm, Michael Huber, Boaz Tirosh, Francesca Levi-Schaffer, Sandro Capellmann, Maike Schwoerer, and Thomas Schubert.

Acknowledgments

K. Maschke-Neuß is acknowledged for excellent technical assistance. Open access funding enabled and organized by Projekt DEAL.

Conflicts of Interest

The authors declare no conflicts of interest.

Data Availability Statement

The data that support the findings of this study are available from the corresponding author upon reasonable request.

Peer Review

The peer review history for this article is available at <https://publons.com/publon/10.1002/eji.202451348>.

References

1. A. Akinleye, P. Avvaru, M. Furqan, Y. Song, and D. Liu, "Phosphatidylinositol 3-kinase (PI3K) Inhibitors as Cancer Therapeutics," *Journal of hematology & oncology* 6, no. 1 (2013): 88, <https://doi.org/10.1186/1756-8722-6-88>.
2. R. Marone, V. Cmiljanovic, B. Giese, and M. P. Wymann, "Targeting Phosphoinositide 3-kinase—Moving towards Therapy," *Biochim Biophys Acta (BBA)—Proteins Proteom* 1784, no. 1 (2008): 159–185, <https://doi.org/10.1016/j.bbapap.2007.10.003>.
3. C. M. Johannessen, JS Boehm, SY Kim, et al., "COT/MAP3K8 Drives Resistance to RAF Inhibition Through MAP Kinase Pathway Reactivation," *Nature* 468, no. 7326 (2010): 968–972, <https://doi.org/10.1038/nature09627>.
4. L. Falchi and S. Verstovsek, "Kit Mutations New Insights and Diagnostic Value," *Immunology and Allergy Clinics of North America* 38, no. 3 (2018): 411–428, <https://doi.org/10.1016/j.jiac.2018.04.005>.
5. A. M. Gilfillan and J. Rivera, "The Tyrosine Kinase Network Regulating Mast Cell Activation," *Immunological Reviews* 228, no. 1 (2009): 149–169, <https://doi.org/10.1111/j.1600-065x.2008.00742.x>.
6. B. M. Vonakis, H. Chen, H. Haleem-Smith, and H. Metzger, "The Unique Domain as the Site on Lyn Kinase for Its Constitutive Association With the High Affinity Receptor for IgE*," *Journal of Biological Chemistry* 272, no. 38 (1997): 24072–24080, <https://doi.org/10.1074/jbc.272.38.24072>.
7. Y. Baba, K. Nishida, Y. Fujii, T. Hirano, M. Hikida, and T. Kurosaki, "Essential Function for the Calcium Sensor STIM1 in Mast Cell Activation and Anaphylactic Responses," *Nature Immunology* 9, no. 1 (2008): 81–88, <https://doi.org/10.1038/nri1546>.
8. R. Sagi-Eisenberg, H. Lieman, and I. Pecht, "Protein Kinase C Regulation of the Receptor-coupled Calcium Signal in Histamine-secreting Rat Basophilic Leukemia Cells," *Nature* 313, no. 5997 (1985): 59–60, <https://doi.org/10.1038/313059a0>.
9. D. E. Cochrane and W. W. Douglas, "Calcium-Induced Extrusion of Secretory Granules (Exocytosis) in Mast Cells Exposed to 48/80 or the Ionophores A-23187 and X-537A," *Pnas* 71, no. 2 (1974): 408–412, <https://doi.org/10.1073/pnas.71.2.408>.
10. M. Huber, "Activation/Inhibition of Mast Cells by Supra-optimal Antigen Concentrations," *Cell Communication and Signaling* 11, no. 1 (2011): 7, <https://doi.org/10.1186/1478-811x-11-7>.

11. V. Hernandez-Hansen, G. A. Mackay, C. A. Lowell, B. S. Wilson, and J. M. Oliver, "The Src Kinase Lyn Is a Negative Regulator of Mast Cell Proliferation," *J Leukoc Biol* 75, no. 1 (2004): 143–151, <https://doi.org/10.1189/jlb.0503224>.
12. S. M. N. de Miranda, T. Wilhelm, M. Huber, and C. N. Zorn, "Differential Lyn-dependence of the SHIP1-deficient Mast Cell Phenotype," *Cell Communication and Signaling* 14, no. 1 (2016): 12, <https://doi.org/10.1186/s12964-016-0135-0>.
13. J. Grootjans, A. Kaser, R. J. Kaufman, and R. S. Blumberg, "The Unfolded Protein Response in Immunity and Inflammation," *Nature Reviews Immunology* 16, no. 8 (2016): 469–484, <https://doi.org/10.1038/nri.2016.62>.
14. C. Hetz, K. Zhang, and R. J. Kaufman, "Mechanisms, Regulation and Functions of the Unfolded Protein Response," *Nat Rev Mol Cell Bio* 21, no. 8 (2020): 421–438, <https://doi.org/10.1038/s41580-020-0250-z>.
15. D. J. Maly and F. R. Papa, "Druggable Sensors of the Unfolded Protein Response," *Nature Chemical Biology* 10, no. 11 (2014): 892–901, <https://doi.org/10.1038/nchembio.1664>.
16. M. Mahameed, T. Wilhelm, O. Darawshi, et al., "The Unfolded Protein Response Modulators GSK2606414 and KIRA6 Are Potent KIT Inhibitors," *Cell death & disease* 10, no. 4 (2019): 300, <https://doi.org/10.1038/s41419-019-1523-3>.
17. D. Rojas-Rivera, T. Delvaeye, R. Roelandt, et al., "When PERK Inhibitors Turn out to be New Potent RIPK1 Inhibitors: Critical Issues on the Specificity and Use of GSK2606414 and GSK2656157," *Cell Death and Differentiation* 24, no. 6 (2017): 1100–1110, <https://doi.org/10.1038/cdd.2017.58>.
18. R. Ghosh, L. Wang, E.S. Wang, et al., "Allosteric Inhibition of the IRE1 α RNase Preserves Cell Viability and Function During Endoplasmic Reticulum Stress," *Cell* 158, no. 3, pp. 534–548, 2014, <https://doi.org/10.1016/j.cell.2014.07.002>.
19. S. K. Meurer, M. Neß, S. Weiskirchen, et al., "Isolation of Mature (Peritoneum-Derived) Mast Cells and Immature (Bone Marrow-Derived) Mast Cell Precursors From Mice," *PLoS ONE* 11, no. 6 (2016): e0158104, <https://doi.org/10.1371/journal.pone.0158104>.
20. M. Sundström, H. Vliagoftis, P. Karlberg, et al., "Functional and Phenotypic Studies of Two Variants of a human Mast Cell Line With a Distinct Set of Mutations in the c-kit Proto-oncogene," *Immunology* 108, no. 1 (2003): 89–97, <https://doi.org/10.1046/j.1365-2567.2003.01559.x>.
21. O. Malbec, K. Roget, C. Schiffer, et al., "Peritoneal Cell-Derived Mast Cells: An in Vitro Model of Mature Serosal-Type Mouse Mast Cells," *Journal of Immunology* 178, no. 10 (2007): 6465–6475, <https://doi.org/10.4049/jimmunol.178.10.6465>.
22. R. Saleh, G. Wedeh, H. Herrmann, et al., "A New human Mast Cell Line Expressing a Functional IgE Receptor Converts to Tumorigenic Growth by KIT D816V Transfection," *Blood* 124, no. 1 (2014): 111–120, <https://doi.org/10.1182/blood-2013-10-534685>.
23. H. Suzuki, M. Takei, M. Yanagida, T. Nakahata, T. Kawakami, and H. Fukamachi, "Early and Late Events in Fc Epsilon RI Signal Transduction in human Cultured Mast Cells," *J Immunol (Baltim, Md : 1950)* 159, no. 12 (1997): 5881–5888.
24. M. W. Pfaffl, "A New Mathematical Model for Relative Quantification in Real-time RT-PCR," *Nucleic Acids Res.* 29, no. 9 (2001): e45–e45, <https://doi.org/10.1093/nar/29.9.e45>.
25. M. Huber, C. D. Helgason, M. P. Scheid, V. Duronio, R. K. Humphries, and G. Krystal, "Targeted Disruption of SHIP Leads to Steel Factor-induced Degranulation of Mast Cells," *Embo Journal* 17, no. 24 (1998): 7311–7319, <https://doi.org/10.1093/emboj/17.24.7311>.
26. K. Gimborn, E. Lessmann, S. Kuppig, G. Krystal, and M. Huber, "SHIP Down-Regulates Fc ϵ R1-Induced Degranulation at Supraoptimal IgE or Antigen Levels," *Journal of Immunology* 174, no. 1 (2005): 507–516, <https://doi.org/10.4049/jimmunol.174.1.507>.
27. O. Larbolette, B. Wollscheid, J. Schweikert, P. J. Nielsen, and J. Wienands, "SH3P7 Is a Cytoskeleton Adapter Protein and Is Coupled to Signal Transduction From Lymphocyte Antigen Receptors," *Molecular and Cellular Biology* 19, no. 2 (1999): 1539–1546, <https://doi.org/10.1128/mcb.19.2.1539>.
28. T. Brummer, W. Elis, M. Reth, and M. Huber, "B Cell Protocols," *Methods Mol Biology Clifton N J* 271 (2004): 189–212, <https://doi.org/10.1385/1-59259-796-3:189>.
29. R. S. Gangwar, H. Pahima, P. G. Puzzovio, and F. Levi-Schaffer, "Methods and Protocols," *Methods in Molecular Biology* 2241 (2021): 221–242, https://doi.org/10.1007/978-1-0716-1095-4_18.
30. H. M. Berman, J. Westbrook, Z. Feng, et al., "The Protein Data Bank," *Nucleic Acids Res.* 28, no. 1 (2000): 235–242, <https://doi.org/10.1093/nar/28.1.235>.
31. N. Eswar, D. Eramian, B. Webb, M.-Y. Shen, and A. Sali, "Structural Proteomics, High-Throughput Methods," *Methods in Molecular Biology* 426 (2008): 145–159, https://doi.org/10.1007/978-1-60327-058-8_8.
32. N. K. Williams, I. S. Lucet, S. P. Klinken, E. Ingley, and J. Rossjohn, "Crystal Structures of the Lyn Protein Tyrosine Kinase Domain in Its Apo- and Inhibitor-bound State*," *Journal of Biological Chemistry* 284, no. 1 (2009): 284–291, <https://doi.org/10.1074/jbc.m807850200>.
33. M. Shen and A. Sali, "Statistical Potential for Assessment and Prediction of Protein Structures," *Protein Science* 15, no. 11 (2006): 2507–2524, <https://doi.org/10.1110/ps.062416606>.
34. M. D. Jacobs, P. R. Caron, and B. J. Hare, "Classifying Protein Kinase Structures Guides Use of Ligand-selectivity Profiles to Predict Inactive Conformations: Structure of Lck/Imatinib Complex," *Proteins: Struct, Funct, Bioinform* 70, no. 4 (2008): 1451–1460, <https://doi.org/10.1002/prot.21633>.
35. R. A. Friesner, J. L. Banks, R. B. Murphy, et al., "Glide: A New Approach for Rapid, Accurate Docking and Scoring. 1. Method and Assessment of Docking Accuracy," *Journal of Medicinal Chemistry* 47, no. 7 (2004): 1739–1749, <https://doi.org/10.1021/jm0306430>.
36. T. A. Halgren, R. B. Murphy, R. A. Friesner, et al., "Glide: A New Approach for Rapid, Accurate Docking and Scoring. 2. Enrichment Factors in Database Screening," *Journal of Medicinal Chemistry* 47, no. 7 (2004): 1750–1759, <https://doi.org/10.1021/jm030644s>.
37. H. J. C. Berendsen, D. van der Spoel, and R. van Drunen, "GROMACS: A Message-passing Parallel Molecular Dynamics Implementation," *Computer Physics Communications* 91, no. 1–3 (1995): 43–56, [https://doi.org/10.1016/0010-4655\(95\)00042-e](https://doi.org/10.1016/0010-4655(95)00042-e).
38. K. Lindorff-Larsen, S. Piana, K. Palmo, et al., "Improved Side-chain Torsion Potentials for the Amber ff99SB Protein Force Field," *Proteins: Struct, Funct, Bioinform* 78, no. 8 (2010): 1950–1958, <https://doi.org/10.1002/prot.22711>.
39. T. Tubiana, J.-C. Carvaillo, Y. Boulard, and S. Bressanelli, "TTClust: A Versatile Molecular Simulation Trajectory Clustering Program With Graphical Summaries," *Journal of Chemical Information and Modeling* 58, no. 11 (2018): 2178–2182, <https://doi.org/10.1021/acs.jcim.8b00512>.
40. M. S. Valdés-Tresanco, M. E. Valdés-Tresanco, P. A. Valiente, and E. Moreno, "gmx_MMPBSA: A New Tool to Perform End-State Free Energy Calculations With GROMACS," *Journal of Chemical Theory and Computation* 17, no. 10 (2021): 6281–6291, <https://doi.org/10.1021/acs.jctc.1c00645>.
41. B. R. Miller, T. D. McGee, J. M. Swails, N. Homeyer, H. Gohlke, and A. E. Roitberg, "MMPBSA.Py: An Efficient Program for End-State Free Energy Calculations," *Journal of Chemical Theory and Computation* 8, no. 9 (2012): 3314–3321, <https://doi.org/10.1021/ct300418h>.
42. A. Wohlsein, S. Uhlig, and C. Martin, "Immediate Allergic Response in Small Airways," *American Journal of Respiratory and Critical Care Medicine* 163, no. 6 (2001): 1462–1469, <https://doi.org/10.1164/ajrccm.163.6.2007138>.

43. F. Martinon, X. Chen, A.-H. Lee, and L. H. Glimcher, "TLR Activation of the Transcription Factor XBP1 Regulates Innate Immune Responses in Macrophages," *Nature Immunology* 11, no. 5 (2010): 411–418, <https://doi.org/10.1038/ni.1857>.
44. K. Fehrenbach, E. Lessmann, C. Zorn, et al., "Steel Factor Enhances Supraoptimal Antigen-Induced IL-6 Production From Mast Cells via Activation of Protein Kinase C- β ," *Journal of Immunology* 182, no. 12 (2009): 7897–7905, <https://doi.org/10.4049/jimmunol.0801773>.
45. J. Kalesnikoff, N. Baur, M. Leitges, et al., "SHIP Negatively Regulates IgE + Antigen-Induced IL-6 Production in Mast Cells by Inhibiting NF- κ B Activity," *Journal of Immunology* 168, no. 9 (2002): 4737–4746, <https://doi.org/10.4049/jimmunol.168.9.4737>.
46. S. Morita, S. A. Villalta, H. C. Feldman, et al., "Targeting ABL-IRE1 α Signaling Spares ER-Stressed Pancreatic β Cells to Reverse Autoimmune Diabetes," *Cell metabolism* 25, no. 4 (2017): 883–897, <https://doi.org/10.1016/j.cmet.2017.03.018>.
47. H. Gorny, A. Mularoni, J.-G. Delcros, C. Freton, J. Preto, and I. Krimm, "Combining Nano-differential Scanning Fluorimetry and Microscale Thermophoresis to Investigate VDAC1 Interaction With Small Molecules," *J Enzym Inhib Med Chem* 38, no. 1 (2022): 2121821, <https://doi.org/10.1080/14756366.2022.2121821>.
48. T. P. Green, M. Fennell, R. Whittaker, et al., "Preclinical Anticancer Activity of the Potent, Oral Src Inhibitor AZD0530," *Mol Oncol* 3, no. 3 (2009): 248–261, <https://doi.org/10.1016/j.molonc.2009.01.002>.
49. K. Yamaki, M. Terashi, S. Ogura, et al., "Anti-allergic Effect of the Src family Kinase Inhibitor saracatinib," *Die Pharm* 75, no. 7 (2020): 339–343, <https://doi.org/10.1691/ph.2020.9949>.
50. Y.-M. Chang, L. Bai, S. Liu, J. C. Yang, H.-J. Kung, and C. P. Evans, "Src family Kinase Oncogenic Potential and Pathways in Prostate Cancer as Revealed by AZD0530," *Oncogene* 27, no. 49 (2008): 6365–6375, <https://doi.org/10.1038/onc.2008.250>.
51. K. N. Chua, L. R. Kong, W. J. Sim, et al., "Combinatorial Treatment Using Targeted MEK and SRC Inhibitors Synergistically Abrogates Tumor Cell Growth and Induces Mesenchymal-epithelial Transition in Non-small-cell Lung Carcinoma," *Oncotarget* 6, no. 30 (2015): 29991–30005, [10.18632/oncotarget.5031](https://doi.org/10.18632/oncotarget.5031).
52. V. Parravicini, M. Gadina, M. Kovarova, et al., "Fyn Kinase Initiates Complementary Signals Required for IgE-dependent Mast Cell Degranulation," *Nature Immunology* 3, no. 8 (2002): 741–748, <https://doi.org/10.1038/ni817>.
53. W. Xiao, H. Nishimoto, H. Hong, et al., "Positive and Negative Regulation of Mast Cell Activation by Lyn via the Fc ϵ RI," *Journal of Immunology* 175, no. 10 (2005): 6885–6892, <https://doi.org/10.4049/jimmunol.175.10.6885>.
54. M. Huber, M. R. Hughes, and G. Krystal, "Thapsigargin-Induced Degranulation of Mast Cells Is Dependent on Transient Activation of Phosphatidylinositol-3 Kinase," *Journal of Immunology* 165, no. 1 (2000): 124–133, <https://doi.org/10.4049/jimmunol.165.1.124>.
55. H. Held, C. Martin, and S. Uhlig, "Characterization of Airway and Vascular Responses in Murine Lungs," *British Journal of Pharmacology* 126, no. 5 (1999): 1191–1199, <https://doi.org/10.1038/sj.bjp.0702394>.
56. I. Kufareva and R. Abagyan, "Type-II Kinase Inhibitor Docking, Screening, and Profiling Using Modified Structures of Active Kinase States," *Journal of Medicinal Chemistry* 51, no. 24 (2008): 7921–7932, <https://doi.org/10.1021/jm8010299>.
57. R. S. K. Vijayan, P. He, V. Modi, et al., "Conformational Analysis of the DFG-Out Kinase Motif and Biochemical Profiling of Structurally Validated Type II Inhibitors," *Journal of Medicinal Chemistry* 58, no. 1 (2015): 466–479, <https://doi.org/10.1021/jm501603h>.
58. S. Odom, G. Gomez, M. Kovarova, et al., "Negative Regulation of Immunoglobulin E-dependent Allergic Responses by Lyn Kinase," *Journal of Experimental Medicine* 199, no. 11 (2004): 1491–1502, <https://doi.org/10.1084/jem.20040382>.
59. M. Kawabuchi, Y. Satomi, T. Takao, et al., "Transmembrane Phosphoprotein Cbp Regulates the Activities of Src-family Tyrosine Kinases," *Nature* 404, no. 6781 (2000): 999–1003, <https://doi.org/10.1038/35010121>.
60. T. Brdička, D. Pavlistová, A. Leo, et al., "Phosphoprotein Associated With Glycosphingolipid-Enriched Microdomains (Pag), a Novel Ubiquitously Expressed Transmembrane Adaptor Protein, Binds the Protein Tyrosine Kinase Csk and Is Involved in Regulation of T Cell Activation," *Journal of Experimental Medicine* 191, no. 9 (2000): 1591–1604, <https://doi.org/10.1084/jem.191.9.1591>.
61. L. Draberova, V. Bugajev, L. Potuckova, et al., "Transmembrane Adaptor Protein PAG/CBP Is Involved in both Positive and Negative Regulation of Mast Cell Signaling," *Molecular and Cellular Biology* 34, no. 23 (2014): 4285–4300, <https://doi.org/10.1128/mcb.00983-14>.
62. E. Ingley, "Src family Kinases: Regulation of Their Activities, Levels and Identification of New Pathways," *Biochim Biophys Acta (BBA)—Proteins Proteom* 1784, no. 1 (2008): 56–65, <https://doi.org/10.1016/j.bbapap.2007.08.012>.
63. M. P. Scheid, M. Huber, J. E. Damen, et al., "Phosphatidylinositol (3,4,5)P3 Is Essential but Not Sufficient for Protein Kinase B (PKB) Activation; Phosphatidylinositol (3,4)P2 Is Required for PKB Phosphorylation at Ser-473 STUDIES USING CELLS FROM SH2-CONTAINING INOSITOL-5-PHOSPHATASE KNOCKOUT MICE*," *Journal of Biological Chemistry* 277, no. 11 (2002): 9027–9035, <https://doi.org/10.1074/jbc.M106755200>.
64. M. Huber, C. D. Helgason, J. E. Damen, et al., "The Role of SHIP in Growth Factor Induced Signalling," *Progress in Biophysics and Molecular Biology* 71, no. 3–4 (1999): 423–434, [https://doi.org/10.1016/S0079-6107\(98\)00049-2](https://doi.org/10.1016/S0079-6107(98)00049-2).
65. H. Hong, J. Kitaura, W. Xiao, et al., "The Src family Kinase Hck Regulates Mast Cell Activation by Suppressing an Inhibitory Src family Kinase Lyn," *Blood* 110, no. 7 (2007): 2511–2519, <https://doi.org/10.1182/blood-2007-01-066092>.
66. D. Korovesis, N. Rufo, R. Derua, P. Agostinis, and S. H. L. Verhelst, "Kinase Photoaffinity Labeling Reveals Low Selectivity Profile of the IRE1 Targeting Imidazopyrazine-Based KIRA6 Inhibitor," *Acs Chemical Biology* 15, no. 12 (2020): 3106–3111, <https://doi.org/10.1021/acscchembio.0c00802>.
67. N. Rufo, D. Korovesis, S. Van Eygen, et al., "Stress-induced Inflammation Evoked by Immunogenic Cell Death Is Blunted by the IRE1 α Kinase Inhibitor KIRA6 Through HSP60 Targeting," *Cell Death and Differentiation* 29, no. 1 (2022): 230–245, <https://doi.org/10.1038/s41418-021-00853-5>.
68. T. Wilhelm, F. Bick, K. Peters, et al., "Infliction of Proteotoxic Stresses by Impairment of the Unfolded Protein Response or Proteasomal Inhibition as a Therapeutic Strategy for Mast Cell Leukemia," *Oncotarget* 9, no. 3 (2017): 2984–3000, [10.18632/oncotarget.23354](https://doi.org/10.18632/oncotarget.23354).
69. P.-H. Nguyen, O. Fedorchenko, N. Rosen, et al., "LYN Kinase in the Tumor Microenvironment Is Essential for the Progression of Chronic Lymphocytic Leukemia," *Cancer Cell* 30, no. 4 (2016): 610–622, <https://doi.org/10.1016/j.ccell.2016.09.007>.

Supporting Information

Additional supporting information can be found online in the Supporting Information section.